# Presence of synchrony-generating hubs in the human epileptic neocortex.

Ágnes Kandrács1,2, Katharina T. Hofer1,2, Kinga Tóth1, Estilla Z. Tóth1, László Entz3, Attila G. Bagó3, Loránd Erőss3, Zsófia Jordán3, Gábor Nagy3, Dániel Fabó3, István Ulbert1,2,3 and Lucia Wittner1,2,3

1. Institute of Cognitive Neuroscience and Psychology, Research Center for Natural Sciences, Hungarian Academy of Sciences, 1117 Budapest, Hungary

2. Department of Information Technology, Pázmány Péter Catholic University, 1083 Budapest, Hungary

3. National Institute of Clinical Neuroscience, 1145 Budapest, Hungary

Correspondence to:

Lucia Wittner

Institute of Cognitive Neuroscience and Psychology,

Research Center for Natural Sciences, Hungarian Academy of Sciences,

1117 Budapest, Magyar tudósok körútja 2. Hungary

tel: +36-1-382-6807

e-mail: wittner.lucia@ttk.mta.hu

ORCID IDs:

Á. Kandrács: 0000-0002-6408-2397

K. T. Hofer: 0000-0002-1626-9288

L. Wittner: 0000-0001-6800-0953

Running head: Bicuculline-induced epileptiform events in human neocortex

Key points summary:

- Initiation of pathological synchronous events such as epileptic spikes and seizures is linked to the hyperexcitability of the neuronal network both in humans and animals.

- Here we show that epileptiform interictal-like spikes and seizures emerged in human neocortical slices by blocking $GABA_A$ receptors, following the disappearance of the spontaneously occurring synchronous population activity.

- Large variability of temporally and spatially simple and complex spikes was generated by tissue from epileptic patients, whereas only simple events appeared in samples from non-epileptic patients.

- Physiological population activity was associated with a moderate level of principal cell and interneuron firing with a slight dominance of excitatory neuronal activity, whereas epileptiform events were mainly initiated by the synchronous and intense discharge of inhibitory cells.

- These results help us to understand the role of excitatory and inhibitory neurons in synchrony generating mechanisms, both in epileptic and non-epileptic conditions.

# Abstract

Understanding the role of different neuron types in synchrony generation is crucial to develop new therapies aiming to prevent hypersynchronous events such as epileptic seizures. Paroxysmal activity was linked to hyperexcitability and to bursting behaviour of pyramidal cells in animals. Human data suggested a leading role of either principal cells or interneurons, depending on the seizure morphology. Here we aimed to uncover the role of excitatory and inhibitory processes in synchrony generation by analysing the activity of clustered single neurons during physiological and epileptiform synchronies in human neocortical slices. Spontaneous population activity was detected with a 24-channel laminar microelectrode in tissue derived from patients with or without preoperative clinical manifestations of epilepsy. This population activity disappeared by blocking $GABA_A$ receptors, and several variations of spatially and temporally simple or complex interictal-like spikes emerged in epileptic tissue, whereas peritumoural slices generated only simple spikes. About half of the clustered neurons participated with an elevated firing rate in physiological synchronies with a slight dominance of excitatory cells. In contrast, more than 90% of the neurons contributed to interictal-like spikes and seizures, and an intense and synchronous discharge of inhibitory neurons was associated to the start of these events. Intrinsically bursting principal cells fired later than other neurons. Our data suggest that a balanced excitation and inhibition characterized physiological synchronies, whereas disinhibition-induced epileptiform events were initiated mainly by non-synaptically synchronized inhibitory neurons. Our results further underline the differences between humans and animal models, and between in vivo and (pharmacologically manipulated) in vitro conditions.

# **Abbreviations**

| | |
|---|---|
| 4-AP | 4-amino-pyridine |
| AP | Action potential |
| BIC | $GABA_A$ receptor antagonist bicuculline |
| CSD | Current source density |
| gran-infra | Granular+infragranular layers |
| HYP | Hypersynchronous activity |
| IIS | Bicuculline-induced interictal-like spike |
| IN | Inhibitory cell |
| LFPg | Local field potential gradient |
| LVF | Low voltage fast activity |
| MUA | Multiple unit activity |
| NoEpi | Patients with no epilepsy |
| NoMed | Patients having one seizure, but they do not need medication |
| PC | Principal cell |
| PDS | Paroxysmal depolarization shift |
| ResEpi | Patients with pharmacoresistant epilepsy |
| SPA | Spontaneous population activity |
| supra-gran | Supragranular+granular layers |
| SWC | Spike and wave complex |
| TreatEpi | Patients with treatable epilepsy |
| UC | Unclassified cell |

# Introduction

Understanding the role of different neuron types in the generation of physiological and pathological synchronies is crucial to identify what makes a brain region predisposed to generate hypersynchronous events, such as epileptic seizures and interictal spikes. Abundant data describe the properties and behaviour of cells and neuronal circuits during epileptic activity in animal models (for reviews see de Curtis & Avanzini, 2001; McCormick & Contreras, 2001; Avoli *et al.*, 2002; Trevelyan *et al.*, 2015), but information about the human cells and disease is considerably less detailed (for reviews see Avoli & Williamson, 1996; Avoli *et al.*, 2005). Knowledge about the cellular and network mechanisms related to synchrony generation mainly derive from the hippocampus and the surrounding medial temporal areas, while the role of different neuron types in synchronisation processes of other neocortical regions remains mainly uncovered. In this study, we explored the firing pattern of human neocortical single cells and microcircuits during synchronizations as well as their possible relationship with epilepsy. We induced epileptic seizures and interictal spikes with the $GABA_A$ receptor antagonist bicuculline (BIC) in human neocortical slices derived from epileptic and tumour patients and compared these pathological events to synchronous population activity spontaneously occurring in physiological solution. We aimed to get insight into the cellular mechanisms by analysing the discharge properties of clustered excitatory and inhibitory neurons during both epileptiform and physiological synchronous events.

The cellular features and the firing pattern of single neurons provide important information about how synchronous events are initiated. The bursting behaviour and the paroxysmal depolarization shift (PDS) of excitatory principal neurons have been linked to the initiation of interictal discharge in animals (for review see de Curtis & Avanzini, 2001). However, in humans, neither in vitro (Prince & Wong, 1981; Avoli & Olivier, 1989; Williamson *et al.*, 2003), nor in vivo early work (Calvin *et al.*, 1973; Ishijima *et al.*, 1975; Wyler *et al.*, 1982; Staba *et al.*, 2002) could find direct evidence for the relation between bursting behaviour and interictal spike generation. More recently, an in vivo study described that cells with modulated firing during interictal spikes have higher burstiness index than non-modulated cells (Keller *et al.*, 2010). In postoperative human neocortical tissue, pharmacologically induced interictal-like activity was used to reveal the cellular properties presumably contributing to the generation of pathological synchronies. The leading role of

excitatory cells and bursting behaviour in the generation of hypersynchronous events was supported by the fact that bursting neurons and depolarization shift were observed in the $Mg^{2+}$-free (Avoli *et al.*, 1995) and in the $K^+$-channel blocker 4-aminopyridine (4-AP, Mattia *et al.*, 1995) models of epileptic activity. In the presence of the $GABA_A$ receptor antagonist bicuculline (BIC, Hwa *et al.*, 1991) interictal-like activity was also reflected as bursts and PDS in human neocortical neurons at the intracellular level. Contrary to the $Mg^{2+}$-free and the 4-AP models, where interictal-like and seizure activity spontaneously emerged, when applying BIC-bath, electrical stimulus was needed to induce epileptiform synchrony.

Cellular synchronization mechanisms leading to the initiation of seizures in epileptic patients were investigated recently, with the aid of intracortical microelectrodes. The dynamic balance of excitation and inhibition characterized the human neocortex in physiological conditions, which broke during epileptic seizures (Dehghani *et al.*, 2016). Increased neuronal firing, up to several minutes before the onset of the seizure was observed both in the neocortex (Truccolo *et al.*, 2011) and the hippocampus (Lambrecq *et al.*, 2017) of epileptic patients. Seizures with different onset patterns were shown to be generated by different mechanisms. The low voltage fast (LVF) activity was the most often detected pattern in the neocortex (Perucca *et al.*, 2014) and was shown to begin with the increased activity of inhibitory interneurons in the medial temporal lobe (Elahian *et al.*, 2018) and other neocortical areas (Dehghani *et al.*, 2016) of humans as well as in animals (for review see Weiss *et al.*, 2019). The hypersynchronous (HYP) seizure onset pattern was observed in patients with mesial temporal lobe epilepsy exclusively (Perucca *et al.*, 2014) and was associated to enhanced excitatory processes both in human (Huberfeld *et al.*, 2011) and experimental epilepsy (Kohling *et al.*, 2016). Preceding the seizures of neocortical origin that spread to the medial temporal lobe, inhibitory but not excitatory neuronal discharge was decreased in the hippocampal formation (Misra *et al.*, 2018). During the course of the seizures heterogeneous firing patterns were detected both in the human hippocampus (Babb *et al.*, 1987) and the neocortex, together with a high ratio of cells increasing their firing rate (Truccolo *et al.*, 2011). Furthermore, spontaneous seizure-like events appeared in neocortical slices derived from epileptic patients, by applying kainate plus carbachol (Florez *et al.*, 2015) as well as in the Mg2+-free model (Avoli *et al.*, 1987; Mattia *et al.*, 1995), which seizures were reflected intracellularly as large depolarizing shift and burst firing (Avoli *et al.*, 1997).

Intracortical microelectrodes recording neuronal activity are implanted only to epileptic patients, and – for obvious ethical reasons – such data cannot be obtained from healthy subjects. Our in vitro model has a considerable advantage compared to in vivo recordings: it has a double

internal control. First, we can compare epileptic tissue to non-epileptic samples derived from tumour patients without clinical manifestations of preoperative epileptic activity. Second, we can compare synchronous activity spontaneously occurring in physiological solution (spontaneous population activity, SPA, Tóth *et al.*, 2018) to epileptiform interictal-like discharges and seizures. SPA emerges in slices derived from patients both with and without epilepsy, shows several crucial differences compared to interictal spikes in vivo, and is considered to be associated to physiological processes (Tóth *et al.*, 2018). However, limitations of the in vitro conditions are evident, i.e. the excised neocortical samples have partially cut internal, and do not possess external connections, and the bath solution is indisputably different from the cerebro-spinal fluid of the living subjects. Although the resulting modified synaptic connections might affect the spontaneous activity of neurons, the double internal control in our model system can help us to identify phenomena related to epileptic conditions.

The aim of this study was to investigate the firing properties of human neocortical neurons during physiological and epileptiform synchronies. Specifically, we wished to describe the role of excitatory and inhibitory cells and circuits in synchrony generation, by comparing the behaviour of neuronal networks and the discharge properties of single cells during SPA and disinhibition-induced interictal spikes and seizures in a human in vitro model of epilepsy.

# Methods

## Ethical Approval

The experiments included in this study were conducted on resected human brain tissue. A written informed consent was obtained from all patients. Our studies conformed to the standards set by the latest revision of the Declaration of Helsinki, except for registration in a database. The procedures were approved by the Regional and Institutional Committee of the National Institute of Clinical Neuroscience, as well as by the Hungarian Ministry of Health and the Research Ethics of Scientific Council of Health (ethical licence number: ETT TUKEB 20680-4/2012/EKU). This study used a partly overlapping patient dataset with our previous work (Tóth *et al.*, 2018).

## Epileptic patients

Samples were resected from 30 epileptic patients (Table 1). We obtained epileptic neocortical tissue from frontal (n=6 patients), temporal (n=17 patients), parietal (n=4 patients) and occipital (n=3 patients) lobes. Most of the patients (n=20) suffered from pharmacoresistant epilepsy (ResEpi, resistant epilepsy) for 28.1±7.3 years on average. As in our previous study (Tóth *et al.*, 2018), we categorized the remaining 10 patients as patients who were either seizure free with appropriate pharmacological treatment (TreatEpi, treatable epilepsy, n=5 patients), or had one (provoked) seizure without the need for medication (NoMed, no need for medication, n=5 patients), and were operated in order to resect their tumour. Ten epileptic patients were diagnosed with cortical dysplasia, 10 patients with tumour of glial origin, 3 patients with carcinoma metastasis. The remaining 7 patients had cavernoma (n=3), gliosis (n=2), haematoma (n=1) and hippocampal sclerosis (n=1, for details see Table 1). Histopathological changes (signs of dysgenesis or tumour infiltration) of the obtained tissue have been verified with Nissl staining, the neuronal marker NeuN-, the astroglial marker glial fibrillary acidic protein- and a specific interneuron marker parvalbumin-immunostaining (Table 1., methods described in (Tóth *et al.*, 2018). Epileptic patients: 17 females, 13 males, age range: 18-68 years, mean±st.dev.: 35.1±13.8 years.

## Non-epileptic patients

Nineteen patients diagnosed with brain tumour but without epilepsy (NoEpi, no epilepsy) were included in this study (Table 1). These patients – as it is stated in their anamnesis – did not show clinical manifestation of epileptic seizure before the date of their brain surgery. Neocortical tissue was resected from tumour patients from frontal (n=7 patients), temporal (n=4 patients), parietal (n=6 patients) and occipital (n=2 patients) lobes. Thirteen patients were diagnosed with tumours of glial origin: glioblastoma (n=10) or anaplastic astrocytoma (n=3). Four patients were operated to remove their carcinoma metastasis, one patient had cavernoma, and one neurocytoma (for details see Table 1). The distance of the obtained neocortical tissue from the tumour (see Table 1) had been assessed by the neurosurgeon, based on magnetic resonance (MR) images, intraoperative pictures and occasionally defined by a navigational system. Non-epileptic patients: 8 females, 11 males, age range: 31-79 years, mean±st.dev.: 58.5±14.6 years.

## Tissue preparation

Tissue was transported from the operating room to the laboratory (located in the same building) in a cold, oxygenated solution containing (in mM) 248 D-sucrose, 26 $NaHCO_3$, 1 KCl, 1 $CaCl_2$, 10 $MgCl_2$, 10 D-glucose and 1 phenol red, equilibrated with 5% $CO_2$ in 95% $O_2$. Neocortical slices of 500 µm thickness were cut with a Leica VT1000S vibratome (RRID:SCR_016495). They were transferred and maintained at 35–37°C in an interface chamber perfused with a standard physiological solution containing (in mM) 124 NaCl, 26 $NaHCO_3$, 3.5 KCl, 1 $MgCl_2$, 1 $CaCl_2$, and 10 D-glucose, equilibrated with 5% $CO_2$ in 95% $O_2$.

## Recordings

The extracellular local field potential gradient (LFPg) recording was obtained as described previously (Tóth *et al.*, 2018). Briefly, we used a 24 contact (distance between contacts: 150 µm) laminar microelectrode (Ulbert *et al.*, 2001; Ulbert *et al.*, 2004a; Ulbert *et al.*, 2004b; Fabó *et al.*, 2008; Wittner *et al.*, 2009), and a custom-made voltage gradient amplifier of pass-band 0.01 Hz to 10 kHz. Signals were digitized with a 32 channel, 16-bit resolution analogue-to-digital converter (National Instruments, Austin TX, USA) at 20 kHz sampling rate, recorded with a home written routine in LabView8.6 (National Instruments,

Austin TX, USA, RRID:SCR_014325). The linear 24 channel microelectrode was placed perpendicular to the pial surface, and slices were mapped from one end to the other at every 300-400 µm.

# Drugs

A-type γ-aminobutyric acid (GABA$_A$) receptor-mediated signalling was suppressed by bicuculline methiodide (BIC, 20 µM or 50 µM), obtained from Tocris Bioscience (Izinta Kft., Hungary). During most of the experiments, 100 ml of solution containing bicuculline was washed into the interface chamber, and 10-minute long epochs were recorded continuously during the whole experiment (control – BIC application – washout). The washout period endured until the reappearance of the spontaneous population activity (SPA). In the absence of a reappearing SPA, the washout persisted for an hour.

# Data analysis

*Analysis of SPAs and BIC-induced events*

The presence or absence of BIC-induced activity was noted in case of every slice. In several cases, only one 10-minute epoch was recorded, but in most of the cases, 3 to 5 epochs were recorded while applying the BIC bath, and the one from the middle/end was chosen for detailed analysis when recurrent BIC-induced events occurred. In case of single events, the file containing the event was analysed.

Data were analysed with the Neuroscan Edit4.5 program (Compumedics Neuroscan, Charlotte, NC, USA), and home written routines for Matlab (The MathWorks, Natick, MA, USA, RRID:SCR_001622) and C++. The microelectrode covered all layers of the neocortex. Usually, channels 1-12 were in the supragranular, channels 13-15 in the granular and channels 16-23 were in the infragranular layers. Channel positions were determined according to the thickness of the neocortex of the given patient and corrected if necessary.

Detection of both spontaneous and BIC-induced population activity was performed on LFPg records after a double Hamming window spatial smoothing and a band-pass filtering between 3 and 30 Hz (zero phase shift, 12 dB/octave). Events larger than two times the standard deviation of the basal activity were detected and included in the analysis. The largest amplitude LFPg peak of simple events was chosen as time zero for averaging and for peri-event time histogram analysis. Two types of synchronous events have been detected during the application

of bicuculline: interictal-like spikes (IISs) and seizure-like events. IISs were further divided into separate groups according to their spatial and temporal complexity. Temporally complex events consisted of multiple LFPg deflections spreading to the same cortical layers. Spatially complex events united waves developing from different locations. In case of complex events (such as complex IISs and seizures), the first LFPg peak on the channel where its amplitude was the largest was chosen as time zero. The location and frequency of the events (see below) were determined in each case. Current source density (CSD; an estimate of population trans-membrane currents), and multiple unit activity (MUA) were calculated from the LFPg using standard techniques (Tóth *et al.*, 2018). The duration of the synchronous events was assessed by two different methods because of the differences in the waveform characteristics of spontaneous and induced synchronous events. The length of spontaneous population activity (SPA) events was measured on the channel displaying the largest LFPg amplitude, at 50% of that amplitude. To have an estimation for the total duration of the SPAs, the halfmax length was multiplied by two. This method could not be applied to bicuculline-induced events, since the length of the LFPg deflections were unequal on the different channels, furthermore, the peak of the deflection was at considerably different time point on the different channels. Therefore, the length of interictal-like spikes (IIS) was calculated using the mean global field power (MGFP) from the channels where the event was present. The MGFP corresponds to the spatial standard deviation of field potential amplitude values obtained with multiple channel recording (Lehmann & Skrandies, 1980; Skrandies, 1990). The average length was calculated at 5% of the maximal MGFP amplitude. In the case of temporally complex IISs, the length of the first component was calculated. The MGFP method could not be applied to SPAs because the LFPg amplitude of these events are low, and therefore the 5% height of the maximal values dropped below the noise level and provided imprecise measurement. The length of BIC-induced seizure-like activities was assessed by manual estimation using the butterfly plot of all channels. In the case of recurring seizures, the butterfly plot was generated from the averaged LFPg, to include all seizure events.

The recurrence frequency was determined in each recording with population events (SPA, IIS, seizure). Note that in case of single epileptiform events, we calculated the recurrence frequency from one, usually 10 minutes long epoch containing the event, although in most of these cases multiple epochs were recorded.

*Time-frequency analysis*

We analysed the ripple and fast ripple components of SPAs, IISs and seizures with the aid of routines written in Matlab, as follows. Original 20 kHz sampling rate records were low pass filtered at 700 Hz and then down-sampled to 2 kHz. Wavelet analysis was applied on epochs from -1 000 ms to 1 047.5 ms for SPAs and from -500 ms to 1 547.5 ms for IISs with the LFPg peak of the SPA/IIS at time zero (detected as described above). In case of seizures, the epoch(s) ranged from -500 ms to 15 883.5 ms. Time-frequency analysis was performed between 0 and 700 Hz on the electrode channels where the SPA/IIS/seizure was present, and baseline corrected to -300 to -100 ms. For each channel, the maximal power change (relative to the baseline) was determined within the range from 130 to 250 Hz (ripple frequency) and 300 to 700 Hz (fast ripple frequency) at time zero (Tóth *et al.*, 2018). The frequencies where the power showed the maximum were also determined. Both the ripple and fast ripple power as well as the frequencies were averaged across the channels; thus, one ripple and one fast ripple power and frequency parameter were determined for each recording. This last step was necessary for the comparison of synchronous activities spreading to different numbers of channels.

*Analysis of the initiation site and the spread of BIC-induced events*

We determined the initiation site, as well as the spreading direction and speed of the BIC-induced events between the neocortical layers. Note, that in our analysis spreading direction refers to interlaminar spread, i. e. propagation across cortical layers. In most cases, the amplitude of the LFPg transient evoked by BIC was large on certain channels but close to baseline (and therefore not detectable) on others. Additionally, an increase in cell firing was associated with the events. To consider both the deflection on the field potential signal as well as the cellular activity, we applied the following method to detect the start of each event on each channel. After applying a 0.5 Hz high-pass filter, we calculated the power of the LFPg signal. The start of the event was defined via a two-step thresholding process. For each recording, we defined two different thresholds. Threshold 1 determined which peaks should be considered as part of the event, whereas threshold 2 determined where the first peak deviates from the baseline. In case threshold 1 was crossed multiple times during one event, the first crossing point was used. We chose threshold 1 manually for each file. We set the threshold to a level ensuring that the first main peak of the BIC-induced events was detected and matched to the previous detection (see above). The variation in MUA and LFPg amplitudes (during the baseline as well as during the BIC-induced event) did not allow a general threshold rule. Note that threshold 1 was not used to detect the BIC-induced events within the recording, as it was

made separately. It was only used within the algorithm to define the beginning of each recording. Starting from threshold 1 time point, the signal was followed to earlier and earlier time points, until it fell below threshold 2 (which was set as low as possible to find the deflection point from the baseline). This time point was used as the start of the event. This process was repeated for every channel and every event. No start was detected for a specific peak if it did not surpass threshold 1. In case of temporally and temporally+spatially complex events, we analysed only the first appearance of the event on a given channel.

The spreading speed of the events across the channels was calculated by dividing the delay between the starting points of the events by the distance between the two electrode contacts in question. This speed value was determined for every channel pair, up to 5 contacts apart. For each event, the speed was calculated by taking the median of these pairwise speed values.

### Cell clustering

Single cells were clustered from records high-pass filtered at 80 Hz or at 500 Hz with the aid of a home-written program for Matlab (Wave Solution). Only neurons with a clear refractory period of at least 1.5 ms were included. Cell clustering during physiological conditions and during the BIC bath was performed separately. Although we made consecutive (usually 10 min long) recordings, the identification of the clusters separated by 30-40 min was very uncertain or even impossible, for the following reason. The cell activity observed in the physiological solution has been considerably changed during the application of BIC. The spontaneously active cells became silent during the application of the drug, while other neurons started to discharge (see more details in the Result section). Changes in the extracellularly recorded action potential (AP) waveform were observed in vivo, during population activity: the amplitude of the APs decreased by ~12% when the firing frequency of the cell was high (Stratton *et al.*, 2012). We considered this phenomenon and clustered our cells accordingly. Furthermore, as others (Merricks *et al.*, 2015), we had difficulties in clustering single units during epileptic seizures because of the distorted action potentials. In these recordings, only cells with relatively high amplitude and recognizable action potential were clustered, whereas small (and noisy) clusters were excluded. During the high frequency oscillatory phases of the seizures cluster detection might be imprecise, therefore conclusions about cell firing during seizure were drawn carefully.

Action potential (AP) waveform analysis and separation of principal cells (PC) and interneurons (IN) was done with the aid of a home written routine in Matlab. Two independent

criteria were used to separate PCs and INs, unbiased by the tissue of origin. The duration of PC APs is significantly higher than that of INs (Wilson & McNaughton, 1993; Csicsvári *et al.*, 1999b). We measured the AP width at the half of the largest LFPg amplitude (half width). The cell was considered to be PC if this value was larger than 0.4 ms, and IN if it was less than 0.2 ms. Cells with AP width between 0.2 and 0.4 ms were defined as unclassified cells (UC). Discharge dynamics was also considered when separating cell types (Barthó *et al.*, 2004; Peyrache *et al.*, 2012). A high peak at 3-10 ms followed by a fast, exponential decay on the autocorrelogram was characteristic to "intrinsically bursting" PCs. If the peak was lacking but there was a sustained firing, or the peak was >10 ms, the cell was considered to be "regular firing" PC. The remaining cells with half widths of >0.4 ms were categorized as PCs with "unclear firing". A slow rise together with a slow decay identified INs. In the hippocampus and neocortex of the living animal, the firing frequency of the cells gives additional information on their identity: PCs have a significantly lower firing rate than INs (Buzsáki & Eidelberg, 1983; Csicsvári *et al.*, 1999a). *In vitro* procedures considerably alter the living conditions of the cells. Therefore, we did not consider this criterion for the identification of the cell type.

Extracellularly recorded very short duration and triphasic action potentials (APs) are indicative of axonally running action potentials, and might be categorized as INs (Robbins *et al.*, 2013). We examined this question in our neuron database and found 6/772 cells (0.8%) with very short half width (<0.1 ms). These cells indeed showed a triphasic waveform, even after transforming the local field potential gradient recording into a "referential-like" recording by referencing all channels to channel 1 (the one at the pial surface).

Analysis of single cell firing was performed with a home written routine in Matlab. The average firing frequency, interevent interval (IEI, event = action potential, AP), and a measure for burstiness (percentage of APs within bursts) were calculated for each cell. Bursts were defined as a set of (at least) three APs within 20 ms. Bursts containing more than three APs could be longer than 20 ms, but each group of three consecutive APs had to be within a 20 ms period. Moreover, the first AP of the burst had to be preceded and the last AP had to be followed by a 20 ms silent period (modified from Staba *et al.*, 2002).

*Cell firing during SPA and BIC-induced events*

We examined the discharge of neurons relative to the LFPg peak of the SPA, IIS and seizure events with two approaches. We made these analyses in each recording containing SPAs, IIS(s) and seizure(s) and single cell firing in slices from the ResEpi (n=15 SPA, n=14 IIS, n=6 seizures) and the NoEpi (n=14 SPA, n=13 IIS, n=3 seizures) groups. First, we aimed

to describe the proportion of single cells which participate in the generation of SPA and IIS events. To do this, we generated PETHs for every cell/SPA, cell/IIS or cell/seizure comparison, with a bin size of 5 ms, from -150 to +50 ms around the LFPg peak of the SPAs and from -400 to +200 ms around the LFPg peak of the IISs and in case of seizures. From these PETHS we calculated the average firing frequency of the neurons during the events as well as during the baseline period. In case of SPAs the time window of the events was from -50 to 50 ms, whereas the baseline ranged from -150 to -50 ms before the LFPg peak of the SPAs. In case of bicuculline-induced population activities the time window of the events was defined between -100 to 200 ms, whereas the baseline ranged from -400 to -100 ms before the LFPg peak of the IISs or the seizures. The normalized firing change was calculated for each cell in the form of $A/(A+B)$, where A is the average firing frequency during the time window of the events and B is the firing frequency during the time window of the baseline. Thus, all values fell between zero and one. A neuron was considered to have an increased firing if its firing change value exceeded 0.6 (which equals to an increase to 150% of its baseline firing rate).

With the second approach, we analysed how excitatory and inhibitory cell types participate in the initiation of SPA, IIS and seizure events. Therefore, we computed combined PETHs for all PC APs, for all IN APs and for all UC APs of the given recording, from -100 to +200 ms around the LFPg peak of the SPAs and -200 to +1000 ms around the LFPg peak of the IISs and seizures. First, we determined in each recording which cell type (PC, IN or UC) starts firing during the SPA/IIS/seizure. Furthermore, we estimated the contribution of the discharge of the different cell types in the initiation of the synchronous events as follows. We calculated the area under the curve of the PC/IN/UC firing of the PETH relative to the total firing during the interval of -50 to +50 ms around the LFPg peak of SPAs, and -100 to +200 ms around the LFPg peak of IISs and seizures.

*Statistics*

Statistical significances were determined using either the program Statistica 13 (Tibco Software Inc. Palo Alto, CA, USA, RRID:SCR_014213) or Matlab. In case of normal distributions (verified with the Kolmogorov-Smirnov & Lilliefors test), a t-test was performed to compare two groups or a One-way ANOVA (with Tukey honest different significance post-hoc test) was performed to compare multiple groups, respectively. If the normality test failed, we used Mann-Whitney U test or Kruskal-Wallis ANOVA for comparing two or multiple groups, respectively. In the main text we provide the mean±standard deviation for easier reading, whereas in the tables we present both the median [1st and 3rd quartiles] as well as the

mean±standard deviation. In order to test for unequal proportions in contingency tables we used http://vassarstats.net. In case of 2x3 contingency tables, the Fisher Exact Probability Test was applied if the total size of the data set was not greater than 300, and the Chi-square test was applied if it exceeded 300.

# RESULTS

*Patient groups*

Patients were distributed into four groups by experienced neurologists (Table 1, (Tóth *et al.*, 2018): 1) patients with pharmacoresistant epilepsy (resistant epilepsy, ResEpi), 2) patients with generalized or focal tonic-clonic seizures who were seizure free with appropriate medication (treatable epilepsy, TreatEpi), 3) patients with one generalized tonic-clonic seizure or with occasional (provoked) seizures, and with no need for medication (no medication, NoMed). These patients were operated in order to resect their tumour, and 4) patients without preoperative seizures (no epilepsy, NoEpi). Glial tumours are known to be highly epileptogenic. Therefore, the anamnesis of tumour patients was carefully checked, and they were asked about their possible epileptic episodes by expert neurologists. Patients with the smallest doubt of having preoperative paroxysmal event(s) were categorized as NoMed (or TreatEpi) patients. Furthermore, preoperative clinical EEG recordings on patients with glial tumours could not confirm the presence of any epileptic activity (Tóth *et al.*, 2018). Patients belonging to the first three groups (ResEpi+TreatEpi+NoMed) were considered to be epileptic, whereas patients in the NoEpi group will be referred to as non-epileptic. To examine changes related to epilepsy, we compared results deriving from the ResEpi group to those from the NoEpi group.

*Emergence of spontaneous activity in physiological bath*

Spontaneous population activity (SPA) was generated in the human epileptic (Fig. 1, Table 2) and non-epileptic neocortex in vitro, in physiological bath solution (see also Köhling *et al.*, 1998; Kerekes *et al.*, 2014; Pallud *et al.*, 2014). Please, note, that SPA designates the totality of recurring synchronous events in a given recording. The number of events per recording varied from 21 to 1229. Single population events will be referred to as 'SPA event'. The emergence rate of SPA was similar in slices derived from epileptic tissue affected vs. not affected by the cortical dysgenesis and it did not differ in samples derived from patients having tumours of glial origin vs. having carcinoma metastasis (Tóth *et al.*, 2018). Occasionally, notably larger and more complex events also spontaneously emerged in tissue from epileptic patients, which were considered to be interictal-like discharges (not shown, n=2/43 slices, (Tóth *et al.*, 2018). We examined n=26 slices with SPA and n=17 slices without SPA derived from 30 epileptic patients, and n=20 slices with SPA and n=6 slices without SPA in tissue

from patients in the NoEpi group (see Table 2). The GABA$_A$ receptor antagonist bicuculline (BIC) abolished the SPA in all cases. In 19 of 25 cases, SPA reappeared when BIC was washed out, whereas 4 slices from ResEpi and 2 slices from the NoEpi group did not generate SPA after the BIC washout. SPA appeared after the BIC washout in 1 slice from the NoMed group, which originally did not generate SPA. Interictal-like discharges spontaneously emerging in physiological bath solution also disappeared during the application of BIC but were not further analysed in this study.

*Bicuculline-induced epileptiform activity*

The application of a BIC bath resulted in the generation of spontaneous epileptiform activity in 27/43 and in 15/26 slices in tissue derived from epileptic and non-epileptic patients, respectively (Table 2, not different, Chi-square test, p=0.87), which disappeared when BIC was washed out. This contrasts with previous results (Schwartzkroin & Haglund, 1986; Hwa *et al.*, 1991), where electrical stimulation was also needed to achieve the emergence of interictal-like spikes in human epileptic neocortical slices during BIC application. Bicuculline-induced activity appeared either as interictal spike (IIS) or as seizure-like activity (Fig. 1.). Note that the term 'interictal-like discharge' is used for spontaneously occurring epileptiform activity in vitro (see above), whereas 'interictal-like spike' (IIS) is used to designate BIC-induced interictal-like activity. Note, that when referring to IIS we mean the totality of interictal-like spike events in a given recording. In the ResEpi group, IISs invaded either the entire width of the neocortex, or were restricted to the supragranular+granular (supra-gran), or to the granular+infragranular (gran-infra) layers (Fig. 2). In all other patient groups, IISs always spread to the entire neocortex (Table 3, Fig. 2D). Based on temporal and spatial complexity, we further classified BIC-induced events as simple or complex events. In the ResEpi group, slices generated different types of IISs (temporally and spatially simple-simple, complex-simple, complex-complex, respectively), whereas in the NoEpi group only simple-simple IISs were detected (Fig. 2, Table 3). Temporally complex IISs consisted of more than one local field potential gradient (LFPg) deflections, with a total duration of up to 5 seconds. Spatially complex IIS events (n=2 activities) were variable in their spatial pattern. In both cases, the first spike of the spatially complex events usually invaded the entire width of the cortex, while during the following spikes of the IISs the supragranular and infragranular layers were differently involved from event to event (Fig. 2E).

Seizures were 15 to 28 sec long, temporally complex epileptiform events, consisting of recurring interictal-like spikes, always invading the entire width of the neocortex (Fig. 3).

The occurrence of seizures was somewhat higher in the ResEpi group (n=7/31, 22.6% of all BIC-induced activities) than in the NoEpi group (n=3/27, 11.1%, significantly not different, Chi-square test, p=0.25). In six slices (five from ResEpi, one from NoEpi), we detected spatially complex seizures, i.e. parts of the seizure pattern were confined only to the supragranular+granular or to the granular+infragranular layers. The other four seizures (n=2 in ResEpi and n=2 in NoEpi slices) were spatially simple events.

Three slices consecutively generated two different activities (one slice in ResEpi: first temporally complex, then simple IISs; one slice in TreatEpi: first IIS, then seizure; one slice in NoEpi: first seizure, then IIS). Furthermore, one slice from ResEpi simultaneously generated two independent and spatially distinct IISs (one supra-gran, and one gran-infra). In this case, the activity emerging in the supragranular layers was similar to SPAs generated in physiological solution. Considering these as distinct activities, we analysed 16 IISs and 7 seizure activities in slices derived from ResEpi, 4 IISs and 1 seizure from TreatEpi, 1 IIS and 1 seizure from NoMed and 13 IISs and 3 seizures from NoEpi.

In summary, we distinguished four types of synchronous activities in the human neocortex, in vitro. SPAs (1) were spontaneously generated in physiological solution in all patient groups, while spontaneous interictal-like discharges (2) appeared only in epileptic patients (not investigated in this study, for details see Tóth *et al.*, 2018). In BIC bath, these two spontaneous activities disappeared, and two other types of synchronies emerged in tissue from both epileptic and non-epileptic patients: IISs (3) and seizures (4). IISs always had a spatially and temporally simple morphology in NoEpi slices, whereas they showed several combinations of spatially and temporally simple and complex manifestations in tissue of ResEpi patients.

*Characterization of SPAs and BIC-induced activities*

To shed light on characteristics related to epileptic mechanisms, in this analysis we compared slices derived from patients in the ResEpi group with those from the NoEpi group. In 12/16 (75%) and 6/13 (46%) cases in the ResEpi and NoEpi groups, respectively, the slices generated recurrent IISs, while in the remaining 4 and 7 cases, respectively, one single IIS event was detected during the entire recording interval (see Methods). The recurrence frequency of SPAs was 0.81±0.54 Hz and 1.08±0.64 Hz in slices derived from ResEpi and NoEpi groups, respectively (Table 4, Fig. 1D, see also Tóth *et al.*, 2018). The recurrence frequency of all IISs was significantly lower than that of SPAs (ANOVA, p<0.0001): in ResEpi slices it was 0.09±0.15 Hz (5.23±9.03 min$^{-1}$), whereas it was 0.02±0.02 Hz (0.88±1.09

min$^{-1}$) in NoEpi slices (ResEpi and NoEpi are significantly not different, t-test, p=0.16). Recurrent seizures emerged only in tissue from epileptic patients (6/7 seizure activity in the ResEpi group, 1/1 in TreatEpi group), while all three seizures generated in slices from NoEpi group were single seizures. The frequency of seizures was very low: 0.007±0.007 Hz (0.42±0.42 min$^{-1}$) in ResEpi slices, and 0.002±0.001 Hz (0.14±0.05 min$^{-1}$) in NoEpi slices (significantly different from SPA, Kruskal-Wallis ANOVA, p<0.0001, but not different from IIS). For easier reading, we give mean±standard deviation (st. dev.) in the main text, but in the Tables both the median [1$^{st}$ and 3$^{rd}$ quartiles] and the mean±st. dev. are provided.

The duration of the different synchronous activity types (SPA, IIS, seizure) were calculated using different methods, thus, they cannot be compared. The average length of the SPAs was 68.8±36.6 ms in ResEpi slices, and 41.6±18.9 ms in NoEpi slices (ResEpi and NoEpi are significantly different, t-test, p<0.01). The average duration of the IISs was 0.36±0.23 s in the ResEpi group and 0.44±0.16 s in the NoEpi group. The average lengths of seizures were 21.75±4.44 s and 24.19±3.48 s in ResEpi and NoEpi groups, respectively (significantly not different between ResEpi and NoEpi, t-test, p=0.42 for IIS length, p=0.43 for seizure length). As the length of the different activity types were calculated with different methods, we do not compare them. However, note the considerable differences (see also Fig. 1).

The LFPg amplitude of SPAs was 38.76±23.67 µV and 26.97±19.03 µV in slices from ResEpi and NoEpi patients, respectively (Table 4). The LFPg amplitude of IISs was about one magnitude higher, than that of SPAs: it was 247.84±240.92 µV in ResEpi and 348.32±322.49 µV in NoEpi slices (IIS significantly different from SPA, ANOVA p<0.0001). The LFPg amplitude of seizures was significantly higher than that of IISs and SPAs: 526.24±259.06 and 847.09±161.46 µV in ResEpi and NoEpi, respectively. Multiple unit activity (MUA) amplitudes during SPAs were 1.28±1.28 µV and 1.27±1.43 µV, while that of IISs was 12.05±8.52 and 22.38±7.49 µV in ResEpi and NoEpi (IIS MUA significantly different from SPA MUA, Kruskal-Wallis ANOVA, p<0.0001), respectively. MUA amplitude was also significantly higher during seizures than during SPA (Kruskal-Wallis ANOVA, p<0.0001): 16.35±5.47 and 37.01±8.59 µV in ResEpi and NoEpi, respectively (Fig. 1D). Interestingly, MUA during both IIS and seizure was significantly higher in NoEpi than in ResEpi slices (Kruskal-Wallis ANOVA, IIS: p<0.05, seizure: p<0.01).

Current source density (CSD) analysis showed that sink-source pairs were restricted to the layers where the LFPg transients were observed (Fig. 1). The most frequent CSD pattern associated to SPA was a sink-source pair, or a source-sink-source triplet in the supragranular

layer, since most of the SPAs were detected in the supragranular layer (see also Köhling *et al.*, 1999). In case of IISs/seizures, sinks and sources were found in all layers of the neocortex, since these activities usually invaded the entire width of the neocortex. As in an earlier study (Köhling *et al.*, 1999), the number and exact location of CSD sinks and sources was variable during both SPAs and epileptiform activities. Sinks and sources usually appeared simultaneously during SPAs, whereas during epileptiform activity the initial sink or source was followed by other sinks and sources. Sink or source or sink-source pair were observed as initial CSD deflection during IISs and seizures. The initial CSD transient could appear in any layer of the neocortex, and we could not find any link between the CSD pattern and the simple or complex nature of the IISs.

The power of the LFPg signal was increased both in the ripple (130-250 Hz) and the fast ripple (300-700 Hz) bands during SPAs, as in our previous study (Tóth *et al.*, 2018). During BIC-induced IISs the power of the signal was elevated in all examined frequency ranges, including ripple and fast ripple bands (Fig. 1, Table 5.). In case of seizures, we could not detect peaks in the ripple and fast ripple bands, since the LFPg power was homogeneously increased in all frequencies. SPAs showed an increased power of high-frequency oscillations (HFOs, both ripple and fast ripple bands) in 17/19 cases in the ResEpi group, in 3/6 cases in the TreatEpi group, whereas ripple and fast ripple power was enhanced in 17/22 and 14/22 cases, respectively, in recordings from NoEpi cases. Ripple and fast ripple power increase during SPAs in the ResEpi group was $3.67 \pm 1.82$ dB and $3.27 \pm 1.57$ dB, respectively, and was similar in the NoEpi group: $3.09 \pm 1.59$ dB and $3.07 \pm 1.60$ dB in ripple and fast ripple bands, respectively. HFO power increased during all IIS activities in recordings from tissue derived from epileptic patients (ResEpi n=15 activities, TreatEpi n=4 and NoMed n=1), whereas it was increased in n=11/13 cases in recordings from the NoEpi group. The power increase of HFOs linked to IISs was significantly higher than during SPA, $12.53 \pm 5.00$ dB and $11.75 \pm 4.67$ dB for ripples and fast ripples, respectively in the ResEpi group, and in NoEpi: $16.05 \pm 3.32$ dB and $15.77 \pm 3.30$ dB for ripples and fast ripples, respectively (both ripple and fast ripple power were significantly different between SPAs and IISs, Mann-Whitney U test, $p < 0.0001$, and NoEpi fast ripple power was significantly different from ResEpi and TreatEpi, One-way ANOVA and Tukey honest significant difference test, $p < 0.05$). The peak frequency of both ripples and fast ripples linked to SPAs or to IISs was lower in the ResEpi than in the NoEpi group, although the differences were not significant (for values see Table 5).

In summary, remarkable differences were observed between the properties of SPAs, IISs and seizures. The recurrence frequency was lower, while the LFPg and MUA amplitudes

and the high frequency power were higher in case of IISs and seizures compared to SPAs. When comparing patient groups, only several features of the synchronies were different. A tendency of generating higher percentage of recurring epileptiform activity was observed in slices from ResEpi compared to NoEpi patients. SPA length and IIS fast ripple power were higher, whereas IIS and seizure MUA were lower in ResEpi than in NoEpi tissue.

*Initiation and propagation of BIC-induced activities across cortical layers*

Most of the IISs (Fig. 2) and all seizures (Fig. 3) invaded the entire width of the neocortex. In cases of spatially complex events, supragranular and infragranular layers were separately activated (Figs. 2E and 3A-B). Supra- and infragranular layers presumably have different roles in interictal spike generation: in vivo spontaneous interictal spikes propagated from other brain areas usually showed an initial activation in the granular or the supragranular areas, whereas de novo generated spikes were initiated in the infragranular layers (Ulbert *et al.*, 2004a). Although propagation from distant sites is excluded in slice preparations, the question arises whether certain layers are more likely to induce synchronous events while others follow, or whether BIC-induced events appear synchronously throughout the entire width of the neocortex. We aimed to explore this question, and therefore we determined the initiation site of the IISs and found several different interlaminar spreading patterns. The initiation site could be in any of the neocortical layers (Fig. 4A): in supragranular layers (n=12 IISs from ResEpi, n=9 from NoEpi), in granular layer (n=4 from ResEpi, n=2 from NoEpi), or in infragranular layers (n=6 from ResEpi, n=2 from TreatEpi). In two recordings (one from ResEpi, the other from NoEpi) we detected two different types of IISs: one was initiated in the supragranular layers and spread to the infragranular layers, and one was generated in the granular layers and spread to the two other layers (Fig. 4E). In all other cases, the initiation layer and spreading directions were stable within one recording. Spatially complex IISs were generated in the granular (n=1) or in infragranular layers (n=1), however, this was not constant during the recording (see Fig. 2E).

We performed a more detailed analysis on how IISs spread across the layers of the neocortex in 12 recordings with recurrent IISs (9 from ResEpi, 1 from TreatEpi, 2 from NoEpi) and in 3 with recurrent seizures (all from ResEpi). In this analysis we included recordings with at least 6 (but up to 166) IIS events, to determine of a precise propagation speed and exclude large bias coming from the eventuality of single epileptiform events. Since seizures occurred with a considerably lower frequency, therefore we analysed recordings with 3 to 5 seizures. Please, note, that our analysis reveals the features of the propagation of epileptic events in the

depth (across the layers) of the neocortex, and not the horizontal spread over larger areas. We determined the initiation time point of every event on each channel, as well as examined its spreading direction and speed (Fig. 4B-E, for details see Methods). In most cases (10/12 recordings), we observed a jitter among the channels over time, i.e. the starting point of the IIS was on different channels in the course of the consecutive events. Furthermore, the activation sequence of the channels was similarly variable as the starting point, although the spreading direction remained constant.

The propagation speed of IISs was also examined within the neocortical column (for details see Methods). We determined a propagation speed for each event and examined how it changes with time. Usually, it was constant throughout the recording (Fig. 4B), however, we found intracortical propagation with increasing (n=3, Fig. 4C) and decreasing (n=1, Fig. 4D) speed as well. The increase/decrease in speed was due either to a faster/slower activation of neighbouring channels (n=1 increased, n=1 decreased) or to the decrease in the jitter observed at channel activation (n=2 increased, Fig. 4B). The average propagation speed of IISs was varying between 19.7 and 98.7 mm/s, with a mean of 51.8±23.7 mm/s in ResEpi and 74.3±39.0 mm/s in NoEpi slices. We observed IISs with low (<30 mm/s) and high (>75 mm/s) propagation speed in both ResEpi and NoEpi slices. In both cases with the two different IIS activation patterns (see above), one IIS had considerably higher propagation speed than the other. When the propagation speed increased over time, it could reach up to a threefold increase (from ~40 to ~120 mm/s). Seizures in ResEpi tissue propagated with a speed of 41.2±12.6 mm/s. The layer of initiation and the propagation speed were not related: high and low speed could be associated to IISs initiated in any layers. We could not find a correlation between the propagation speed of the IISs and the aetiology of the patients. High, medium and low speed IISs were observed in ResEpi slices derived from patients with dysplasia, tumour or hippocampal sclerosis. High speed IISs were detected in NoEpi slices derived from patients with carcinoma metastasis or with glial tumour.

Our observation is that bicuculline-induced population events can be generated in any cortical layer. Although the starting channel can change over time, the layer of initiation remains stable. The direction and the speed of the intracortical propagation were usually constant, with some exceptions when propagation speed increased or decreased throughout the recording.


*Firing characteristics of single cells*

In this analysis we included all files with population activity (SPA/IIS/seizure) and

single cell activity from the ResEpi and NoEpi groups. Recordings lacking either synchronous event or single ells were excluded, and only ResEpi and NoEpi recordings were compared to focus on epilepsy-related characteristics. We clustered 384 and 349 single cells in recordings from ResEpi and NoEpi groups, respectively. In ResEpi 193 single units (from 16 slices derived from 13 patients, with an average±standard deviation of 10.9±6.7 neurons/slice and 13.4±7.9 neurons/patient) were clustered in control conditions and 191 (from 18 slices derived from 15 patients, with 11.1±5.4 neurons/slice and 14.0±11.2 neurons/patient) during application of BIC, whereas in NoEpi 182 cells (from 14 slices derived from 11 patients with 13.3±12.7 neurons/slice and 16.9±20.8 neurons/patient) in control and 167 (from 14 slices derived from 10 patients, with 11.6±7.6 neurons/slice and 16.3±14.7 neurons/patient) in a solution containing BIC (Table 6). In most cases we clustered cells from one slice per patient, but in samples derived from five patients (2 ResEpi and 3 NoEpi patients) we could analyse two or three slices per patients. To increase the number of cell/IIS comparison, we included two further recordings from the TreatEpi group with high numbers of neurons (n=39 single cells in 2 slices) and IIS events. When comparing cellular discharge in physiological conditions and in BIC-bath, we noticed several patterns of firing change. In physiological solution, spontaneously discharging cells were observed mainly in the supragranular and the infragranular layers. During BIC application, the majority of these cells became silent, while other – previously not detected – spontaneously discharging neurons appeared on other recording channels (Fig. 5). We noticed that cells located in the granular layer often showed a very characteristic bursting-like firing pattern (Fig. 5A, C), which was very rarely seen in control conditions. In several cases in BIC-bath, neurons discharged only during the BIC-induced events and were silent between the events (Fig. 5B, n=1/12 with seizures in ResEpi, and n=7/33 with IISs, 6 from ResEpi, 1 from NoEpi), even if spontaneous neuronal activity was observed in physiological solution before the application of the BIC.

We separated excitatory principal cells (PC) and inhibitory interneurons (IN) based on their action potential shape and firing patterns (for details see Methods, Fig 5D-E). For the analysis of the cellular properties in relation with epilepsy, cells in the TreatEpi group were excluded, and only ResEpi and NoEpi were compared. The ratio of detectable (i.e. spontaneously firing) PCs was higher than that of INs during physiological conditions in tissue from both epileptic and non-epileptic patients: ResEpi: 39.4% PC, 19.7% IN and 40.9% unclassified cells (UC), NoEpi: 27.5% PC, 21.4% IN and 51.1% UC. Interestingly, this ratio changed in BIC bath, i.e. spontaneously discharging INs were more abundant than PCs, both in ResEpi and NoEpi tissue (Table 6, ResEpi: 14.7% PC, 36.1% IN and 49.2% UC; NoEpi:

18.0% PC, 33.5% IN and 48.5% UC, cell proportions in BIC are significantly different from that in control, both in ResEpi and NoEpi, p<0.0001 and p<0.05, respectively, Chi-square test). The ratio of intrinsically bursting PCs was low in both patient groups: in ResEpi 1.6% in control condition and 2.1% in BIC, in NoEpi 2.7% in physiological and 1.8% in BIC bath.

The firing frequency of neurons was somewhat higher in ResEpi tissue than in NoEpi tissue (Table 6). Furthermore, in physiological bath, INs showed a slightly higher average firing frequency than PCs, both in ResEpi and NoEpi slices. Differences in the firing frequency were not significantly different. In BIC bath, the overall firing frequency of the cells did not change, although the vast majority of the cells fired with a very high frequency during the BIC-induced events. This latter phenomenon was reflected in the significantly increased burstiness together with the decrease of the interevent interval of all neuron types during the application of BIC, compared to control conditions (for values and significances see Table 6).

In summary, other neurons were spontaneously active during physiological conditions than in BIC bath. Higher numbers of PCs than INs were spontaneously firing in physiological bath, while this ratio was reversed during the application of BIC. The average firing frequency remained unchanged in BIC bath, with a modified firing pattern: the neurons intensely discharged during the epileptiform events and tended to be more silent between the events.

*Neuronal firing related to synchronous activity*

We aimed to examine the mechanisms of synchrony initiation in the human neocortex, therefore we investigated the activity of single neurons during SPAs, IISs and seizures with several approaches.

First, we verified whether a combined discharge of single cells forms a build-up period before SPAs and BIC-induced events, as in the rodent hippocampus before interictal-like events (Menendez de la Prida *et al.*, 2002; Cohen *et al.*, 2006; Wittner & Miles, 2007). Neuronal firing preceding the SPA events was only occasionally seen. Build-up discharge was observed in 7/21 SPAs in ResEpi and in 6/22 SPAs in NoEpi tissue. The existence of the neuronal discharge before the events was rare within one recording, we noted cellular firing before in 1.6±4.9% of the events in ResEpi and only in 0.1±0.1% of the events in NoEpi tissue.

In recordings with IISs, we observed neuronal firing before the events more often: in 7/17 IISs in the ResEpi and in 7/14 IISs in the NoEpi group (Fig. 4A). We detected cell firing before the events in 21.9±40.6% of the events in the ResEpi, and in 30.3±41.2% in the NoEpi group. Increased neuronal firing was observed up to several minutes before seizures in

epileptic patients both in the neocortex (Truccolo *et al.*, 2011) and the hippocampus (Lambrecq *et al.*, 2017). In contrast, during BIC-induced seizures in vitro, cells were always silent before the seizures (n=7 in ResEpi and n=3 in NoEpi), they started to fire abruptly with the first large LFPg component, and usually showed an intense firing at the late, decreasing component (Fig 3C).

*Single cell firing during SPA*

We examined how single cells behaved during SPAs emerging in physiological solution. To get insight into the synchronization mechanisms, we analysed how neurons change their firing during SPAs, by computing the firing change during the events compared to baseline periods (see Methods, Fig 6A). The normalized firing change of all cells was 0.55±0.30 in ResEpi, (n=136 cells in 15 files with SPA) and 0.64±0.31 in NoEpi tissue (n=124 cells in 14 files with SPA, Fig 6B). Single cells were considered to have an increased firing if their normalized firing increase was equal or more than 0.6 (an increase to at least 150%). Slightly more cells increased their firing during SPA in NoEpi (56%) than in ResEpi (39%) slices (Table 7). We did not find significant differences between the cell types, similar percentages of PCs, INs and UCs showed increased discharge during both ResEpi and NoEpi SPA, with comparable normalized firing change. As the activity of burst firing PCs was related to epilepsy and to epileptiform discharges (Connors, 1984), we separately investigated the activity of this special neuron group. Out of the three bursting PCs detected in ResEpi tissue, the firing of two was increased during SPA, while one remained unchanged. In the NoEpi tissue 2/5 bursting PCs increased their firing during SPA (Table 7, Fig 6A).

Next, we examined how excitatory or inhibitory cells participate in the generation of SPAs. Therefore, we analysed the combined firing of all PCs, all INs and all UCs within each recording with SPA both in ResEpi and NoEpi tissue. In line with the above finding, i.e. about half of the cells showed increased firing during SPA, in several cases no clear population firing enhancement was visible during SPA (n=6/15 SPA in ResEpi and 5/14 SPA in NoEpi tissue, Fig 6C-D). Furthermore, we could not determine a constant sequence of cell type activation, as both excitatory or inhibitory neuronal population could start firing while the other followed (Fig 6C-D). In ResEpi INs started to discharge in n=2 cases while PCs started in n=4 cases, in NoEpi both INs and PCs started to fire in three and three cases. UCs or all cell types together were also observed to elevate their discharge at the beginning of the SPAs. To estimate the impact of the firing of PC and IN populations on SPA generation, we calculated the ratio of PC and IN action potentials relative to all single cell firing during SPAs (see Methods). We

found that 32.7±36.7% of the APs derived from PCs, while 24.3±30.8% came from INs during ResEpi SPA, and 31.7±33.2% from PCs and 15.4±21.5% from INs during NoEpi SPA. The contribution of bursting PCs was 3.9±13.1% in ResEpi and 7.2±14.7% in NoEpi slices in the overall firing (Table 8, Figure 7E).

In summary, about half of the cells increased their firing rate during SPA, both in ResEpi and NoEpi tissue. No significant differences were found between patient groups or cell types. Either PCs or INs could start discharging at the beginning of the SPAs, while the other cell types followed. PCs contribute to the overall firing slightly more than INs.

*Single cell firing during BIC-induced activity*

Results focussing on the role of excitatory and inhibitory cell types in the initiation of synchronies related to epilepsy provided controversial data. When GABA$_A$ receptors were blocked by BIC in slice preparations, bursting pyramidal cells were shown to induce interictal-like events both in the hippocampus (Cohen *et al.*, 2006; Wittner & Miles, 2007), and the neocortex (Connors, 1984) of rodents. On the other hand, interneurons discharged before pyramidal cells during spontaneously occurring interictal-like activity in the human subiculum, in vitro (Pallud *et al.*, 2014). Furthermore, a heterogeneous cell population showed a complex interplay during interictal spikes in the human neocortex of epileptic patients (Keller *et al.*, 2010). The beginning of seizures was also associated to glutamatergic (Huberfeld *et al.*, 2011) or GABAergic (Elahian *et al.*, 2018) processes, depending on the seizure morphology. To clarify the role of excitatory and inhibitory neuronal populations in the generation of epileptiform activity, we determined the normalized firing increase of neurons, as well as the contribution of PCs and INS during IISs and seizures and compared these data to those related to SPAs.

The normalized firing change during IISs was significantly higher than during SPA (Kruskal-Wallis ANOVA, p<0.001), and even higher during seizures (significantly different, p<0.001), both in ResEpi and NoEpi slices (ResEpi IIS: 0.86±0.31, seizure: 0.97±0.12; NoEpi IIS: 0.95±0.17, seizures: 1.0±0.0, see Table 7). During ResEpi IIS and seizures 86% and 99% of the cells increased their firing rate, respectively (SPA-IIS-seizure significantly different, Chi square test, p<0.001), whereas during NoEpi IIS and seizures 95% and 100%, respectively (SPA-IIS-seizure significantly different, Fisher Exact Test, p<0.001). Similar to SPAs, no differences were seen between cell types: similar proportions of PCs, INs and UCs showed increased firing with similar values of normalized firing increase (for values and significances

see Table 7). Concerning intrinsically bursting PCs, 3/4 and 3/3 were found to increase their firing rate in ResEpi and NoEpi IIS, respectively. No bursting PCs were clustered in the recordings with seizures.

Next, we performed PETHs by computing the discharge of all PC, all IN and all UC cells separately, in each recording with IISs and seizures, as well as examined the timing of intrinsically bursting PCs, separately. To increase the number of IIS examined, beside the 14 recordings in ResEpi and the 13 in NoEpi group, we included two more recordings with high numbers of IIS events from the TreatEpi group. Contrary to our expectations, i.e. (bursting) PCs initiate IISs (Connors, 1984; Wittner & Miles, 2007), we found that in most cases INs fired earlier than PCs in our human neocortical disinhibition model of epilepsy. IN firing preceded the discharge of other cell types (PC and UC) during IISs in 7/14 recordings in the ResEpi group and in 5/13 recordings in the NoEpi group (Fig. 7). PCs began the discharge pattern in three and in two cases in ResEpi and NoEpi slices, respectively. In all the remaining recordings (n=4 in ResEpi, n=2/2 in TreatEpi and n=6 in NoEpi), UC cells started to fire during the IISs, while other cells followed (ResEpi and NoEpi significantly not different, Fisher Exact Test, p>0.6). Four intrinsically bursting PCs were discharging during IISs in ResEpi, three in TreatEpi and three in NoEpi slices. All ResEpi, all TreatEpi and one NoEpi bursting PCs fired later than the INs detected in the same recording (Fig. 7B, C), and the remaining two bursting PCs in the NoEpi tissue discharged later than all UCs (n=7) of the same recording (Fig. 7D).

Similar to IIS, INs tended to discharge before PCs during the initial phase of seizures. In the ResEpi group, INs started to fire together with UCs in 3/6 cases, while PCs followed. PCs and UCs initiated seizures in 2/6 and 1/6 cases, respectively. In the NoEpi group, in all cases (n=3) INs started to discharge (once together with UCs) while PC followed.

We analysed how a neuronal population of a given slice generates SPA and epileptiform activity. As we observed SPA in the majority of the slices before inducing IIS/seizure, we verified whether the same neuron type initiated SPA and IIS/seizure in the same slice. In samples from ResEpi patients we observed similar initiator neuron type in 2/14 slice, and in 2/13 in NoEpi slices. In the remaining slices different cell types initiated SPAs than IISs/seizures.

To see the contribution of excitatory and inhibitory discharge in epileptiform synchronies, we calculated the percentage of APs given by PCs and INs during the initial firing of IISs and seizures. As in the ratio of clustered PCs and INs, we found a switch in excitatory and inhibitory contribution in the firing compared to SPAs, only 16.5±29.0% and 12.2±15.4% of the APs came from PCs in ResEpi and NoEpi IIS, whereas 43.4±34.3% and 46.4±29.1% of

the APs derived from INs, respectively (Table 8). Burst firing PCs contributed to the total firing in 1.7±3.7% in ResEpi and in 1.1±3.6% in NoEpi IIS. In case of seizures, the values for PCs and INs were not different from IISs: ResEpi seizures: 18.8±30.9% from PCs, 32.2±17.7% from INs, NoEpi seizures: 3.6±4.3% from PCs, 59.9±26.8% from INs.

Next, we analysed the correlation between the propagation speed of IISs (see above) and the cellular contribution. Unclassified cells discharged at the initial phase of the two NoEpi and one TreatEpi slice examined for propagation speed. In the ResEpi slices we could not find any relation between highly contributing cell type and propagation speed. High speed IISs were initiated by either INs or all cell types together, medium speed IISs were initiated by PCs, or IN+UCs or PC+UCs. Low speed IISs were initiated by PCs, INs or by IN+UCs.

We experienced that almost all neurons, independently from their type, increased their firing rate during IISs and seizures. In most of the cases, INs started to discharge at the onset of the epileptic synchronies, while other neurons followed, but PCs and UCs were also found to fire at the initial phase of the hypersynchronous events. During both IISs and seizures INs provided higher ratio of action potentials to the overall firing than PCs, which is in contrast to SPAs where PCs contributed more than INs.

# **Discussion**

*Synchrony generating hubs in the human neocortex*

When applying the GABA$_A$ receptor antagonist BIC, tissue slices in the ResEpi group tended to generate seizures and IISs more often, and with somewhat higher recurrence frequency, than slices derived from the NoEpi group. Furthermore, we detected several combinations of temporally and spatially simple and complex IISs in ResEpi tissue, whereas only simple-simple IISs were recorded in NoEpi samples, spreading to all layers of the neocortex. In slices from the ResEpi group spatially more restricted IISs were also observed (supragranular or infragranular IISs), and supragranular and infragranular neuron populations were separately activated during temporally and spatially complex IISs (Fig 2E). This suggests that epileptic neural circuits – possibly as a consequence of the epileptic reorganization – are more likely to initiate hypersynchronous events than non-epileptic networks. In the human epileptic neocortex smaller neuronal populations of the cortical network were also able to generate IISs, compared to NoEpi tissue. These delimited neural circuits, similar to the hippocampal "hub" cells or cell populations (Feldt Muldoon *et al.*, 2013; Bui *et al.*, 2015), or the "pathologically interconnected neuron clusters" (Bragin *et al.*, 2000) of epileptic rodents, might act as initiators for the generation of hypersynchronous events.

*Effects of BIC on neuronal firing*

Considerably higher numbers of inhibitory interneurons were detected in a perfusion solution containing BIC, compared to physiological conditions, where the majority of the spontaneously firing cells were excitatory principal cells. This might be explained by the difference in the synaptic input of the different cell types. In the rodent hippocampus, the proportion of inhibitory synapses arriving at CA1 pyramidal cells was 5.3% (Megias *et al.*, 2001). All interneuron types examined so far received higher ratio of inhibitory inputs than pyramidal cells: 6.4% of the boutons forming synapses with parvalbumin-containing interneurons were GABAergic (which cell type received a considerably high number of glutamatergic boutons), 29.4% of the synapses terminating on calbindin-positive interneurons were inhibitory, 20.7% were GABAergic on calretinin-positive (Gulyás *et al.*, 1999) and 35.85% on cholecystokinin-containing interneurons (Mátyás *et al.*, 2004). As GABA$_A$ receptors are blocked by BIC (Simmonds, 1980), the transmission of fast GABAergic hyperpolarizing potentials from inhibitory cells to their postsynaptic targets is largely reduced, and consequently, cells are released from their usual inhibition. Since the proportion of the

GABAergic input terminating on INs is higher, than on PCs, this might result in the more pronounced increase in excitability of these cells, and thus in the appearance of high numbers of spontaneously active INs. Although the above data are derived from the rodent hippocampus, comparable synaptic input proportions might characterize the human neocortical neurons as well.

The possibility that bicuculline distorts the shape of action potentials cannot be excluded and might also account for the high proportions of INs detected in the disinhibited human neocortex. BIC was shown to reduce the afterhyperpolarization phase of the action potentials, but not the duration of the depolarization and repolarization phases (Seutin *et al.*, 1997). Since we used the length of the action potential at the half of the maximal amplitude to distinguish between excitatory and inhibitory cell types (and not the peak-to-through duration which would be distorted by bicuculline), this possibility is very unlikely.

*Synchrony generating mechanisms in the human neocortex*

In this study we investigated the excitatory and inhibitory processes during presumably physiological synchrony such as SPA (Tóth *et al.*, 2018), as well as during interictal-like spikes and seizures. Considerable differences were observed between SPA and BIC-induced epileptiform activities. SPAs had a clearly lower level of synchrony, than pathological events: only half of the cells increased their firing, and cells had a normalized firing increase of about 0.50-0.60. As expected, IISs were more synchronized events, with about 90% of cells with enhanced firing and a normalized firing increase of ~0.85-0.95. Seizures displayed the highest degree of synchrony, involving practically all cells, which had a normalized firing increase of 0.97-1.00. The role of the different excitatory and inhibitory neuron types in the generation of hypersynchronous events has been long investigated but remained a debated question. Both excitatory bursting pyramidal cells (Connors, 1984) and inhibitory interneurons (Pallud *et al.*, 2014) were found to initiate interictal-like discharges in neocortical slices, whereas neurons responded with diverse firing patterns to interictal spikes in the neocortex of epileptic patients (Keller *et al.*, 2010). Similarly, seizure onset was linked to both excitatory (Huberfeld *et al.*, 2011) and inhibitory (Elahian *et al.*, 2018) processes, depending on the morphology of the seizure. We found that the role of excitatory and inhibitory neurons was different in physiological vs. pathological synchronies. PCs had a higher contribution to the overall firing than INs during SPA (PC: ~32% vs. IN: 15-24%), which reversed during epileptiform activities (both IIS and seizure): INs contributed with

higher percentages to the overall firing than PCs (IIS PC: ~15% vs. IN: ~45%; seizure PC: ~3-18% vs. IN: ~32-60%).

We have to note, that the relatively low occurrence rate of the seizure-like activities and the heterogeneous origin of the tissue samples do not allow us to draw far-reaching concusions about the generation of seizures. A methodological difficulty further complicates the investigation of seizure initiation mechanisms. High electrical activity of the brain, such as an epileptic seizure was shown to modify the properties of extracellular action potentials used for cell clustering, and therefore deteriorated the identification of single cells (Merricks *et al.*, 2015). Merricks et al. (2015) recorded using a multielectrode array with large (~400 µm) interelectrode distance, which corresponds to multiple but single electrode recording. Higher spatial electrode density, like tetrode configuration largely improves the identification of single cell action potentials (Gray *et al.*, 1995). We used a multiple channel electrode with a considerably smaller contact distance (150 µm) allowing a better neuron separation than the above study, but we have to note that our clustered cells discharging during seizures are possibly less precise than neurons detected during other conditions. However, the impact of seizure activity on cell clustering is probably similar in case of PCs and INs, and thus our results about the contribution of the different cell types in the initiation of seizures is a valid assumption.

Based on our findings, we propose that SPAs emerge on the basis of a complex and balanced interaction of excitatory and inhibitory networks. This refers to in vivo physiological conditions in human patients, where a dynamic balance of excitation and inhibition characterized the neocortex (Dehghani *et al.*, 2016). The higher impact of PC firing suggests that excitatory networks might have a leading role (which is not necessarily required for the initiation itself) in this type of synchrony.

Epileptiform IISs and seizures appeared spontaneously, when the application of BIC artificially impaired the balance of excitation and inhibition. These hypersynchronous events involved the vast majority of neurons, and the elevated contribution of IN discharge indicates that they were mainly initiated by inhibitory cells.


*Non-synaptic mechanisms to synchronise cellular activity in the disinhibited neocortex*

We found an intense inhibitory cell discharge at the initial phase of BIC-induced epileptiform events (both IISs and seizures). This raises the question, how the neocortical

circuit can be synchronised if the downstream step of the interneuronal firing (i.e. the transmission through postsynaptic GABA$_A$ receptors) is blocked. Our results, that inhibitory cell firing can lead these synchronisation processes implies that non-synaptic cellular interactions are also involved in the generation of disinhibition-induced hypersynchronous events in the human neocortex. Non-synaptic interactions are transmitted through gap junctions, ephaptic effects, the change in extracellular ions (Jefferys, 1995) and through neuropeptides (for review see van den Pol, 2012). Indeed, BIC-induced epileptic activity is regulated by a neural network connected through gap junctions in the guinea pig brain preparation (de Curtis *et al.*, 1998). Gap junctions specifically connect parvalbumin-positive interneurons in the rat neocortex (Galarreta & Hestrin, 1999), which cell type is thought to "control rhythm" in physiological conditions (Freund & Katona, 2007). Neurons are not in close apposition in the human neocortex, and so, ephaptic effect is possibly less important than in the hippocampus, where it can clearly participate in synchronisation processes (Dudek *et al.*, 1986). Increase in extracellular K$^+$ concentration has been shown to enhance the excitability – and the spontaneous discharge rate – of hippocampal neurons (Cohen & Miles, 2000), and thus, high level of extracellular K$^+$ is commonly used to induce epileptiform activity in vitro. But the increase in K$^+$ concentration during disinhibition-induced epileptic activity is rather the consequence of the paroxysmal discharges, since it starts to elevate after the onset of the epileptic bursts (Heinemann *et al.*, 1977). Neuropeptides present in inhibitory cells might also modify the activity of other neurons in the presence of BIC. However, neuropeptides – such as neuropeptide Y (NPY), somatostatin, cholecystokinin, etc. – mainly act by reducing neurotransmitter release from the presynaptic terminals (for review see van den Pol, 2012). Especially, NPY was found to decrease both glutamate and GABA release in the rat neocortex, which explained its antiepileptic effect (Bacci *et al.*, 2002). In summary, electrical connection through gap junctions is the most probable non-synaptic mechanism to synchronise interneuron populations in the human neocortex when GABA$_A$ receptors are blocked, while the others seem to be unlikely. This theory has to be tested in the future.


*Human disease vs. models*

BIC-induced epileptic activities were hypersynchronous events, with the synchronous and intense firing of INs during the initial phase. This was an unexpected finding in case of IISs, since in the same BIC model in rodents, synchrony was shown to develop due to the loss of inhibitory control, and neurons were recruited into spikes via recurrent excitatory

pathways (Miles & Wong, 1987). Excitatory bursting PCs were demonstrated to initiate BIC-induced IISs both in neocortical (Connors, 1984) and hippocampal (Cohen *et al.*, 2006; Wittner & Miles, 2007) slices of rodents. This clearly differs in the disinhibited human neocortex, as all intrinsically bursting PCs were found to discharge later than other cells of the same recording. Data about the generation mechanisms of interictal spikes in epileptic patients are very sparse. About half of the extracellularly detected cells participated in the spikes both in the neocortex (Ishijima *et al.*, 1975; Keller *et al.*, 2010) and the hippocampus (Alvarado-Rojas *et al.*, 2013), with a heterogeneous firing pattern (Keller *et al.*, 2010). PCs and INs were not distinguished in these studies, thus information about excitatory and inhibitory signalling in the generation of interictal spikes in epileptic patients is lacking.

Seizures occurring in human neocortical slices in our BIC model consisted of continuously recurring interictal-like spikes, lasting for 15 to 28 seconds. This morphology resembles to in vivo seizures composed of periodic spikes (Perucca *et al.*, 2014) or spike and wave complexes (Truccolo *et al.*, 2014). Seizures with hypersynchronous spike onset in animal models (Salami *et al.*, 2015; Kohling *et al.*, 2016), as well as preictal discharges in human slices (Huberfeld *et al.*, 2011) were related to excitatory processes. In contrast, the dominance of inhibitory cell firing characterized the onset of BIC-induced seizures (such as that of IISs) in our experiments, which mechanism was seen at low voltage fast activity seizures in epileptic patients (Dehghani *et al.*, 2016; Elahian *et al.*, 2018) and in rodents (Gnatkovsky *et al.*, 2008).

The above differences and inconsistencies found in our experiments and in the different publications might be explained by species differences and/or by the different conditions and methods used, as well as the different cortical regions investigated. Bursting pyramidal cells in the guinea pig (Connors, 1984) vs. interneuronal firing in human neocortical slices (our results) initiating BIC-induced interictal spikes points to species differences. Pharmacological manipulations and in vitro circumstances clearly differ from in vivo conditions (BIC-induced vs. spontaneously occurring epileptic activity in patients). The largely reduced GABAergic neurotransmission in vitro eventuates in different synchronisation mechanisms than those of the intact brain, where the dynamic balance of excitation and inhibition breaks and transforms into epileptic seizure (Dehghani *et al.*, 2016). Furthermore, differences in the examined cortical region might also account for the dissimilarities observed in the results. The generation mechanism of hypersynchronous spikes (Huberfeld *et al.*, 2011) and seizures (Salami *et al.*, 2015) was related to excitatory processes in the 3-layered hippocampal formation, while epileptiform activity with similar morphology, i.e. manifested

as single or multiple spikes were associated to an enhanced interneuronal firing in the 6-layered neocortex (our data). Our results suggest that the disinhibition model of epileptic activity shows considerable differences compared to the human disease. Furthermore, as we showed here, the same disinhibition model operates with different mechanisms in human tissue compared to rodents.

# **Conclusions**

Our data indicate that physiological synchronous population events emerged on the basis of a complex interaction between excitatory and inhibitory networks in the human neocortex. The disinhibition of the neural circuit – through the impairment of the excitation-inhibition balance – resulted in the spontaneous generation of hypersynchronous epileptiform activities, such as IISs and seizures. IISs were uniform in NoEpi samples: they always invaded the entire neocortex and were simple events. In tissues derived from epileptic patients IISs were heterogeneous, either spreading to the entire width of the neocortex or restricted to a subset of layers, and several variations of temporally and spatially simple and complex events were also detected. This suggests that smaller neuron populations are able to generate epileptiform activity in the neocortex of epileptic patients than in peritumoural tissue, which might act as synchrony initiator circuits.

In the generation of physiological events excitatory neuron firing might have a leading role, whereas epileptiform activity was mainly initiated by inhibitory cell discharge. This latter finding suggests that non-synaptic mechanisms might also play an important role in synchrony generation, most presumably the electrical connection between certain interneuron populations through their gap junctions. Our results about hypersynchronous events initiated by inhibitory cells differ from results obtained in animal models or in epileptic patients, and implies that different neural mechanisms might be activated in the disinhibition model, than in the human disease. Therefore, conclusions should be drawn carefully when using pharmacologically induced, in vitro models of epilepsy, by considering the limits of extrapolation from model to disease and from animals to humans.

# Additional Information Section

## Author contributions

Data acquisition was performed in the National Institute of Clinical Neuroscience, Budapest, Hungary (NICN) and in the Institute of Cognitive Neuroscience and Psychology, Research Center for Natural Sciences, Hungarian Academy of Sciences, Budapest, Hungary (ICNP RCNS HAS). Brain tissue resection and the electrophysiological experiments were conducted in the NICN, the anatomical experiments were performed in the ICNP RCNS HAS. Data analysis, interpretation of the results and article writing were done in the ICNP RCNS HAS. Á.K., K.T.H., K.T., E.Zs.T., L.Entz, A.G.B., L.Erőss, Zs.J. and G.N. participated in acquisition, analysis and interpretation of data, and in revising critically the work for intellectual content. D.F., I.U. and L.W. made the conception or design of the work, participated in acquisition, analysis and interpretation of data, as well as drafting the work and revising it critically for intellectual content. All authors approved the final version of the manuscript. All authors agree to be accountable for all aspects of the work in ensuring that questions related to the accuracy or integrity of any part of the work are appropriately investigated and resolved. All persons designated as authors qualify for authorship, and all those persons who qualify for authorship are listed.

## Competing Interests

The authors have no conflict of interest to declare.

# References

Alvarado-Rojas C, Lehongre K, Bagdasaryan J, Bragin A, Staba R, Engel J, Jr., Navarro V & Le Van Quyen M. (2013). Single-unit activities during epileptic discharges in the human hippocampal formation. *Front Comput Neurosci* **7,** 140.

Avoli M, D'Antuono M, Louvel J, Kohling R, Biagini G, Pumain R, D'Arcangelo G & Tancredi V. (2002). Network and pharmacological mechanisms leading to epileptiform synchronization in the limbic system in vitro. *Prog Neurobiol* **68,** 167-207.

Avoli M, Hwa G, Louvel J, Kurcewicz I, Pumain R & Lacaille JC. (1997). Functional and pharmacological properties of GABA-mediated inhibition in the human neocortex. *Can J Physiol Pharmacol* **75,** 526-534.

Avoli M, Louvel J, Drapeau C, Pumain R & Kurcewicz I. (1995). GABAA-mediated inhibition and in vitro epileptogenesis in the human neocortex. *J Neurophysiol* **73,** 468-484.

Avoli M, Louvel J, Pumain R & Köhling R. (2005). Cellular and molecular mechanisms of epilepsy in the human brain. *Prog Neurobiol* **77,** 166-200.

Avoli M, Louvel J, Pumain R & Olivier A. (1987). Seizure-like discharges induced by lowering [Mg2+]o in the human epileptogenic neocortex maintained in vitro. *Brain Res* **417,** 199-203.

Avoli M & Olivier A. (1989). Electrophysiological properties and synaptic responses in the deep layers of the human epileptogenic neocortex in vitro. *J Neurophysiol* **61,** 589-606.

Avoli M & Williamson A. (1996). Functional and pharmacological properties of human neocortical neurons maintained in vitro. *Prog Neurobiol* **48,** 519-554.

Babb TL, Wilson CL & Isokawa-Akesson M. (1987). Firing patterns of human limbic neurons during stereoencephalography (SEEG) and clinical temporal lobe seizures. *Electroencephalogr Clin Neurophysiol* **66,** 467-482.

Bacci A, Huguenard JR & Prince DA. (2002). Differential modulation of synaptic transmission by neuropeptide Y in rat neocortical neurons. *Proc Natl Acad Sci U S A* **99,** 17125-17130.

Barthó P, Hirase H, Monconduit L, Zugaro M, Harris KD & Buzsáki G. (2004). Characterization of neocortical principal cells and interneurons by network interactions and extracellular features. *J Neurophysiol* **92,** 600-608.

Bragin A, Wilson CL & Engel J, Jr. (2000). Chronic epileptogenesis requires development of a network of pathologically interconnected neuron clusters: a hypothesis. *Epilepsia* **41 Suppl 6,** S144-152.

Bui A, Kim HK, Maroso M & Soltesz I. (2015). Microcircuits in Epilepsy: Heterogeneity and Hub Cells in Network Synchronization. *Cold Spring Harb Perspect Med* **5**.

Buzsáki G & Eidelberg E. (1983). Phase relations of hippocampal projection cells and interneurons to theta activity in the anesthetized rat. *Brain Res* **266,** 334-339.

Calvin WH, Ojemann GA & Ward AA, Jr. (1973). Human cortical neurons in epileptogenic foci: comparison of inter-ictal firing patterns to those of "epileptic" neurons in animals. *Electroencephalogr Clin Neurophysiol* **34,** 337-351.

Cohen I, Huberfeld G & Miles R. (2006). Emergence of disinhibition-induced synchrony in the CA3 region of the guinea pig hippocampus in vitro. *J Physiol* **570,** 583-594.

Cohen I & Miles R. (2000). Contributions of intrinsic and synaptic activities to the generation of neuronal discharges in in vitro hippocampus. *J Physiol* **524 Pt 2,** 485-502.

Connors BW. (1984). Initiation of synchronized neuronal bursting in neocortex. *Nature* **310,** 685-687.

Csicsvári J, Hirase H, Czurkó A, Mamiya A & Buzsáki G. (1999a). Fast network oscillations in the hippocampal CA1 region of the behaving rat. *J Neurosci* **19,** RC20.

Csicsvári J, Hirase H, Czurkó A, Mamiya A & Buzsáki G. (1999b). Oscillatory coupling of hippocampal pyramidal cells and interneurons in the behaving Rat. *J Neurosci* **19,** 274-287.

de Curtis M & Avanzini G. (2001). Interictal spikes in focal epileptogenesis. *Prog Neurobiol* **63,** 541-567.

de Curtis M, Manfridi A & Biella G. (1998). Activity-dependent pH shifts and periodic recurrence of spontaneous interictal spikes in a model of focal epileptogenesis. *J Neurosci* **18,** 7543-7551.

Dehghani N, Peyrache A, Telenczuk B, Le Van Quyen M, Halgren E, Cash SS, Hatsopoulos NG & Destexhe A. (2016). Dynamic Balance of Excitation and Inhibition in Human and Monkey Neocortex. *Sci Rep* **6,** 23176.

Dudek FE, Snow RW & Taylor CP. (1986). Role of electrical interactions in synchronization of epileptiform bursts. *Adv Neurol* **44,** 593-617.

Elahian B, Lado NE, Mankin E, Vangala S, Misra A, Moxon K, Fried I, Sharan A, Yeasin M, Staba R, Bragin A, Avoli M, Sperling MR, Engel J, Jr. & Weiss SA. (2018). Low-voltage fast seizures in humans begin with increased interneuron firing. *Ann Neurol* **84,** 588-600.

Fabó D, Maglóczky Z, Wittner L, Pék A, Erőss L, Czirják S, Vajda J, Sólyom A, Rásonyi G, Szűcs A, Kelemen A, Juhos V, Grand L, Dombovári B, Halász P, Freund TF, Halgren E, Karmos G & Ulbert I. (2008). Properties of in vivo interictal spike generation in the human subiculum. *Brain* **131,** 485-499.

Feldt Muldoon S, Soltesz I & Cossart R. (2013). Spatially clustered neuronal assemblies comprise the microstructure of synchrony in chronically epileptic networks. *Proc Natl Acad Sci U S A* **110,** 3567-3572.

Florez CM, McGinn RJ, Lukankin V, Marwa I, Sugumar S, Dian J, Hazrati LN, Carlen PL, Zhang L & Valiante TA. (2015). In vitro recordings of human neocortical oscillations. *Cereb Cortex* **25,** 578-597.

Freund TF & Katona I. (2007). Perisomatic inhibition. *Neuron* **56,** 33-42.

Galarreta M & Hestrin S. (1999). A network of fast-spiking cells in the neocortex connected by electrical synapses. *Nature* **402,** 72-75.

Gnatkovsky V, Librizzi L, Trombin F & de Curtis M. (2008). Fast activity at seizure onset is mediated by inhibitory circuits in the entorhinal cortex in vitro. *Ann Neurol* **64,** 674-686.

Gray CM, Maldonado PE, Wilson M & McNaughton B. (1995). Tetrodes markedly improve the reliability and yield of multiple single-unit isolation from multi-unit recordings in cat striate cortex. *J Neurosci Methods* **63,** 43-54.

Gulyás AI, Megias M, Emri Z & Freund TF. (1999). Total number and ratio of excitatory and inhibitory synapses converging onto single interneurons of different types in the CA1 area of the rat hippocampus. *J Neurosci* **19,** 10082-10097.

Heinemann U, Lux HD & Gutnick MJ. (1977). Extracellular free calcium and potassium during paroxsmal activity in the cerebral cortex of the cat. *Exp Brain Res* **27,** 237-243.

Huberfeld G, Menendez de la Prida L, Pallud J, Cohen I, Le Van Quyen M, Adam C, Clémenceau S, Baulac M & Miles R. (2011). Glutamatergic pre-ictal discharges emerge at the transition to seizure in human epilepsy. *Nat Neurosci* **14,** 627-634.

Hwa GG, Avoli M, Oliver A & Villemure JG. (1991). Bicuculline-induced epileptogenesis in the human neocortex maintained in vitro. *Exp Brain Res* **83,** 329-339.

Ishijima B, Hori T, Yoshimasu N, Fukushima T & Hirakawa K. (1975). Neuronal activities in human epileptic foci and surrounding areas. *Electroencephalogr Clin Neurophysiol* **39,** 643-650.

Jefferys JG. (1995). Nonsynaptic modulation of neuronal activity in the brain: electric currents and extracellular ions. *Physiol Rev* **75,** 689-723.

Keller CJ, Truccolo W, Gale JT, Eskandar E, Thesen T, Carlson C, Devinsky O, Kuzniecky R, Doyle WK, Madsen JR, Schomer DL, Mehta AD, Brown EN, Hochberg LR, Ulbert I, Halgren E & Cash SS. (2010). Heterogeneous neuronal firing patterns during interictal epileptiform discharges in the human cortex. *Brain* **133,** 1668-1681.

Kerekes BP, Tóth K, Kaszás A, Chiovini B, Szadai Z, Szalay G, Pálfi D, Bagó A, Spitzer K, Rózsa B, Ulbert I & Wittner L. (2014). Combined two-photon imaging, electrophysiological and anatomical investigation of the human neocortex, in vitro. *Neurophotonics* **1,** 011013(011011-011010).

Kohling R, D'Antuono M, Benini R, de Guzman P & Avoli M. (2016). Hypersynchronous ictal onset in the perirhinal cortex results from dynamic weakening in inhibition. *Neurobiol Dis* **87,** 1-10.

Köhling R, Lucke A, Straub H, Speckmann EJ, Tuxhorn I, Wolf P, Pannek H & Oppel F. (1998). Spontaneous sharp waves in human neocortical slices excised from epileptic patients. *Brain* **121 ( Pt 6),** 1073-1087.

Köhling R, Qu M, Zilles K & Speckmann EJ. (1999). Current-source-density profiles associated with sharp waves in human epileptic neocortical tissue. *Neuroscience* **94,** 1039-1050.

Lambrecq V, Lehongre K, Adam C, Frazzini V, Mathon B, Clemenceau S, Hasboun D, Charpier S, Baulac M, Navarro V & Le Van Quyen M. (2017). Single-unit activities during the transition to seizures in deep mesial structures. *Ann Neurol* **82,** 1022-1028.

Lehmann D & Skrandies W. (1980). Reference-free identification of components of checkerboard-evoked multichannel potential fields. *Electroencephalogr Clin Neurophysiol* **48,** 609-621.

Mattia D, Olivier A & Avoli M. (1995). Seizure-like discharges recorded in human dysplastic neocortex maintained in vitro. *Neurology* **45,** 1391-1395.

Mátyás F, Freund TF & Gulyás AI. (2004). Convergence of excitatory and inhibitory inputs onto CCK-containing basket cells in the CA1 area of the rat hippocampus. *Eur J Neurosci* **19,** 1243-1256.

McCormick DA & Contreras D. (2001). On the cellular and network bases of epileptic seizures. *Annu Rev Physiol* **63,** 815-846.

Megias M, Emri Z, Freund TF & Gulyas AI. (2001). Total number and distribution of inhibitory and excitatory synapses on hippocampal CA1 pyramidal cells. *Neuroscience* **102,** 527-540.

Menendez de la Prida L, Benavides-Piccione R, Sola R & Pozo MA. (2002). Electrophysiological properties of interneurons from intraoperative spiking areas of epileptic human temporal neocortex. *Neuroreport* **13,** 1421-1425.

Merricks EM, Smith EH, McKhann GM, Goodman RR, Bateman LM, Emerson RG, Schevon CA & Trevelyan AJ. (2015). Single unit action potentials in humans and the effect of seizure activity. *Brain* **138,** 2891-2906.

Miles R & Wong RK. (1987). Inhibitory control of local excitatory circuits in the guinea-pig hippocampus. *J Physiol* **388,** 611-629.

Misra A, Long X, Sperling MR, Sharan AD & Moxon KA. (2018). Increased neuronal synchrony prepares mesial temporal networks for seizures of neocortical origin. *Epilepsia* **59,** 636-649.

Pallud J, Le Van Quyen M, Bielle F, Pellegrino C, Varlet P, Labussiere M, Cresto N, Dieme MJ, Baulac M, Duyckaerts C, Kourdougli N, Chazal G, Devaux B, Rivera C, Miles R, Capelle L & Huberfeld G. (2014). Cortical GABAergic excitation contributes to epileptic activities around human glioma. *Science translational medicine* **6,** 244ra289.

Perucca P, Dubeau F & Gotman J. (2014). Intracranial electroencephalographic seizure-onset patterns: effect of underlying pathology. *Brain* **137,** 183-196.

Peyrache A, Dehghani N, Eskandar EN, Madsen JR, Anderson WS, Donoghue JA, Hochberg LR, Halgren E, Cash SS & Destexhe A. (2012). Spatiotemporal dynamics of neocortical excitation and inhibition during human sleep. *Proc Natl Acad Sci U S A* **109,** 1731-1736.

Prince DA & Wong RK. (1981). Human epileptic neurons studied in vitro. *Brain Res* **210,** 323-333.

Robbins AA, Fox SE, Holmes GL, Scott RC & Barry JM. (2013). Short duration waveforms recorded extracellularly from freely moving rats are representative of axonal activity. *Frontiers in neural circuits* **7,** 181.

Salami P, Levesque M, Gotman J & Avoli M. (2015). Distinct EEG seizure patterns reflect different seizure generation mechanisms. *J Neurophysiol* **113,** 2840-2844.

Schwartzkroin PA & Haglund MM. (1986). Spontaneous rhythmic synchronous activity in epileptic human and normal monkey temporal lobe. *Epilepsia* **27,** 523-533.

Seutin V, Scuvee-Moreau J & Dresse A. (1997). Evidence for a non-GABAergic action of quaternary salts of bicuculline on dopaminergic neurones. *Neuropharmacology* **36,** 1653-1657.

Simmonds MA. (1980). Evidence that bicuculline and picrotoxin act at separate sites to antagonize gamma-aminobutyric acid in rat cuneate nucleus. *Neuropharmacology* **19,** 39-45.

Skrandies W. (1990). Global field power and topographic similarity. *Brain Topogr* **3,** 137-141.

Staba RJ, Wilson CL, Bragin A, Fried I & Engel J, Jr. (2002). Sleep states differentiate single neuron activity recorded from human epileptic hippocampus, entorhinal cortex, and subiculum. *J Neurosci* **22,** 5694-5704.

Stratton P, Cheung A, Wiles J, Kiyatkin E, Sah P & Windels F. (2012). Action potential waveform variability limits multi-unit separation in freely behaving rats. *PLoS One* **7,** e38482.

Tóth K, Hofer KT, Kandrács A, Entz L, Bagó A, Erőss L, Jordán Z, Nagy G, Sólyom A, Fabó D, Ulbert I & Wittner L. (2018). Hyperexcitability of the network contributes to synchronization processes in the human epileptic neocortex. *J Physiol* **596,** 317-342.

Trevelyan AJ, Muldoon SF, Merricks EM, Racca C & Staley KJ. (2015). The role of inhibition in epileptic networks. *J Clin Neurophysiol* **32,** 227-234.

Truccolo W, Ahmed OJ, Harrison MT, Eskandar EN, Cosgrove GR, Madsen JR, Blum AS, Potter NS, Hochberg LR & Cash SS. (2014). Neuronal ensemble synchrony during human focal seizures. *J Neurosci* **34,** 9927-9944.

Truccolo W, Donoghue JA, Hochberg LR, Eskandar EN, Madsen JR, Anderson WS, Brown EN, Halgren E & Cash SS. (2011). Single-neuron dynamics in human focal epilepsy. *Nat Neurosci* **14,** 635-641.

Ulbert I, Halgren E, Heit G & Karmos G. (2001). Multiple microelectrode-recording system for human intracortical applications. *J Neurosci Methods* **106,** 69-79.

Ulbert I, Heit G, Madsen J, Karmos G & Halgren E. (2004a). Laminar analysis of human neocortical interictal spike generation and propagation: current source density and multiunit analysis in vivo. *Epilepsia* **45 Suppl 4,** 48-56.

Ulbert I, Maglóczky Z, Erőss L, Czirják S, Vajda J, Bognár L, Tóth S, Szabó Z, Halász P, Fabó D, Halgren E, Freund TF & Karmos G. (2004b). In vivo laminar electrophysiology co-registered with histology in the hippocampus of patients with temporal lobe epilepsy. *Exp Neurol* **187,** 310-318.

van den Pol AN. (2012). Neuropeptide transmission in brain circuits. *Neuron* **76,** 98-115.

Weiss SA, Staba R, Bragin A, Moxon K, Sperling M, Avoli M & Engel J, Jr. (2019). "Interneurons and principal cell firing in human limbic areas at focal seizure onset". *Neurobiol Dis* **124,** 183-188.

Williamson A, Patrylo PR, Lee S & Spencer DD. (2003). Physiology of human cortical neurons adjacent to cavernous malformations and tumors. *Epilepsia* **44,** 1413-1419.

Wilson MA & McNaughton BL. (1993). Dynamics of the hippocampal ensemble code for space. *Science* **261,** 1055-1058.

Wittner L, Huberfeld G, Clémenceau S, Erőss L, Dezamis E, Entz L, Ulbert I, Baulac M, Freund TF, Maglóczky Z & Miles R. (2009). The epileptic human hippocampal cornu ammonis 2 region generates spontaneous interictal-like activity in vitro. *Brain* **132,** 3032-3046.

Wittner L & Miles R. (2007). Factors defining a pacemaker region for synchrony in the hippocampus. *J Physiol* **584,** 867-883.

Wyler AR, Ojemann GA & Ward AA, Jr. (1982). Neurons in human epileptic cortex: correlation between unit and EEG activity. *Ann Neurol* **11,** 301-308.
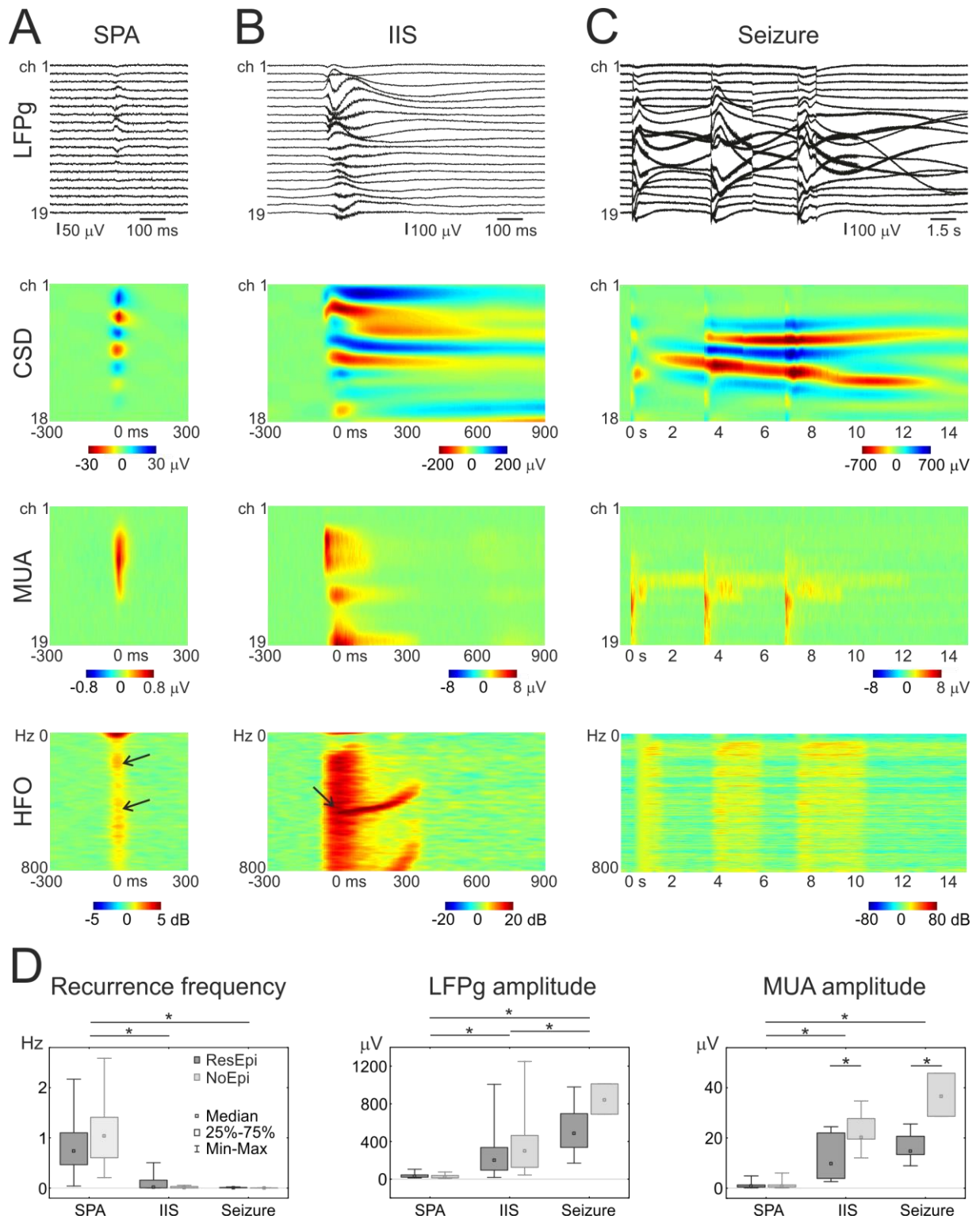
*Figure 1. Different population activities in the human neocortex, in vitro.*

A-C) Spontaneous population activity (A, SPA) was generated in human neocortical slices derived from patients with or without epilepsy. During the application of the $GABA_A$ receptor antagonist bicuculline (BIC) spontaneous epileptiform activity emerged, such as interictal-like spikes (B, IIS) or seizures (C). SPAs were usually restricted to a subset of neocortical layers

(see on the local field potential gradient, LFPg traces, current source density, CSD and multiple unit activity, MUA maps), whereas IISs and seizures mainly invaded the entire width of the neocortex. IISs and seizures were larger LFPg and CSD amplitude events, with highly increased neuronal firing (higher MUA amplitude), than SPAs. An increased high frequency oscillatory (HFO) activity in the ripple and fast ripple bands (arrows) was characteristic to SPAs, while during IIS and seizures all frequency bands showed an increased power. On this IIS example we detected a long-lasting fast ripple power increase (arrow). The CSD, MUA and HFO heat maps were computed from SPA and IIS averages, while that of epileptic seizure was performed from one single event. Note the different colour and time scales.

D) The recurrence frequency of SPAs was significantly higher, while the LFPg and MUA amplitudes were significantly lower than that of epileptiform events. Furthermore, MUA amplitudes of NoEpi IIS and seizure were significantly higher than that of ResEpi slices. *p<0.05
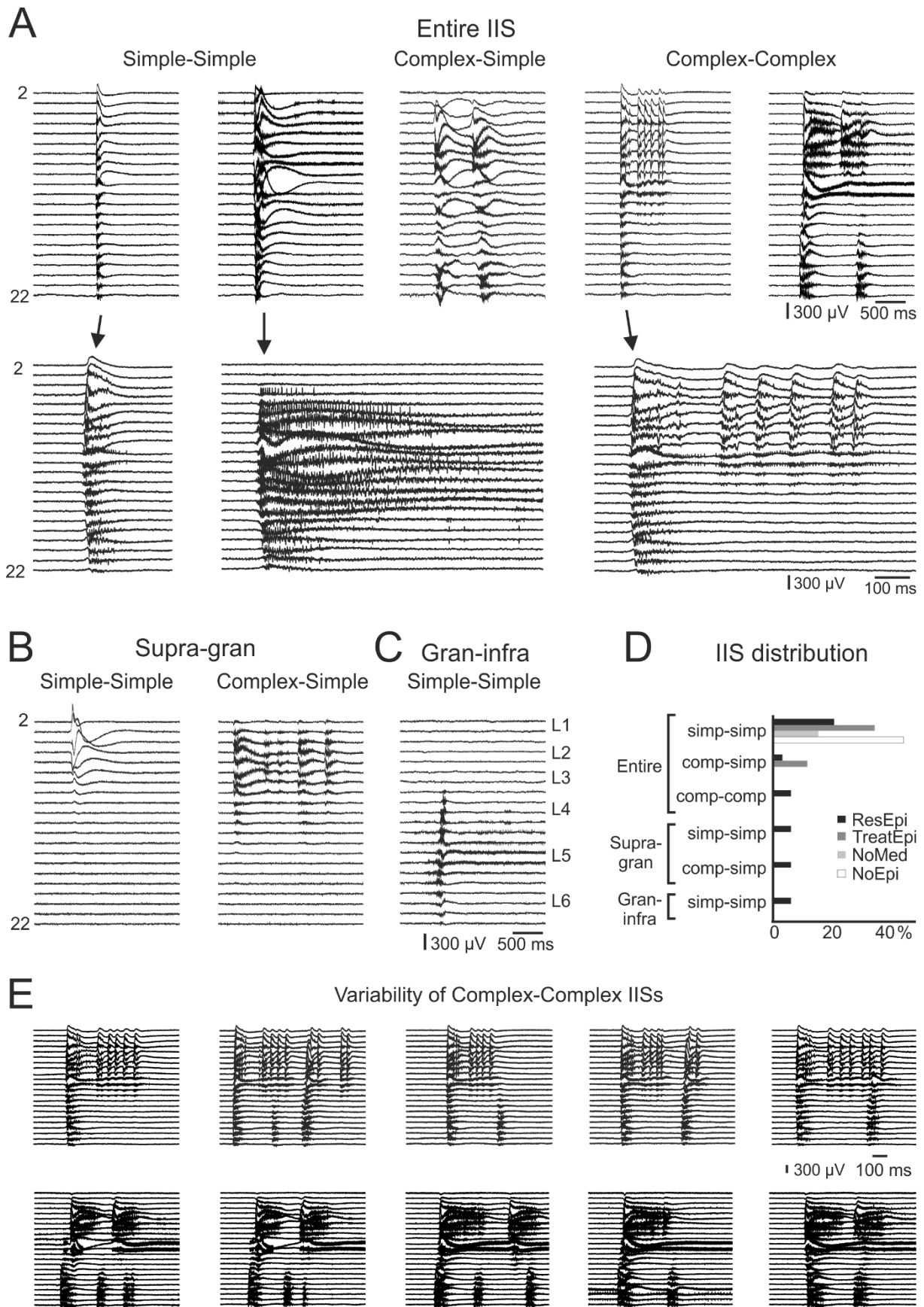
*Figure 2. Different types of BIC-induced IISs in the human neocortex*

IISs were grouped based on their temporal and spatial complexity. In most cases IISs spread to the entire width of the neocortex (A), but spatially more restricted IISs (B, C) were also detected in ResEpi samples. Temporally complex events consisted of more than one LFPg deflection, such as complex-simple (A, B) and complex-complex IISs (A). Three of the IIS events shown on (A) are magnified in the second row. Note the difference in the length of the two simple-simple events (same time scale). In case of spatially complex events the neocortical layers were separately activated: complex-complex events on (A), with a high variability from event to event (E). Subfigure (D) shows the distribution of the different types of IISs in relation with the patient groups. In NoEpi tissue only simple-simple IISs were detected, whereas in ResEpi samples several different types of IISs occurred. Supra-gran: supragranular+granular, Gran-infra: granular+infragranular, simp: simple, comp: complex

**A** ResEpi - Complex-Complex
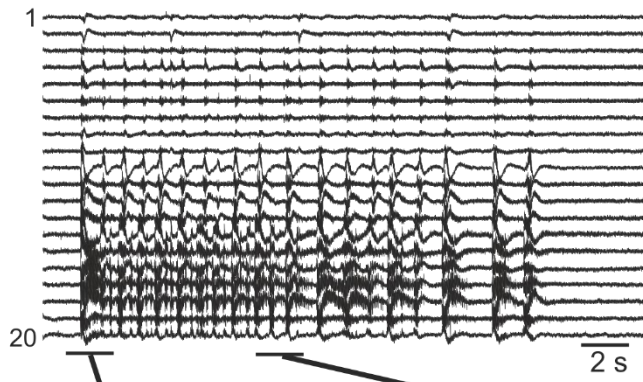
**B**
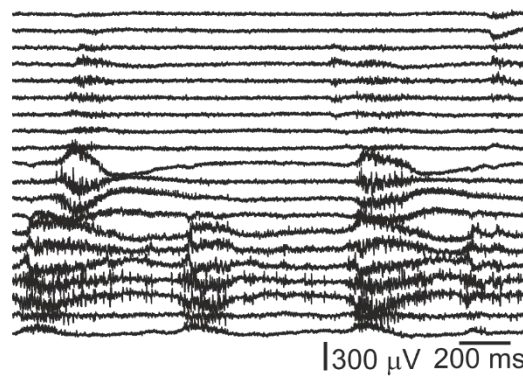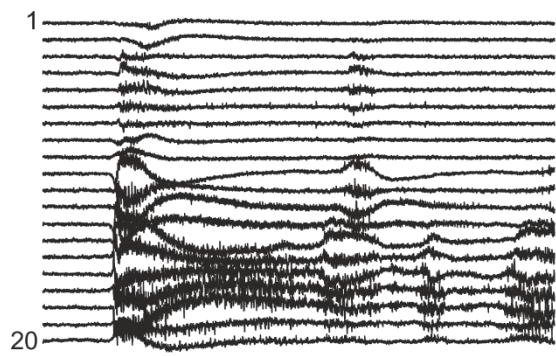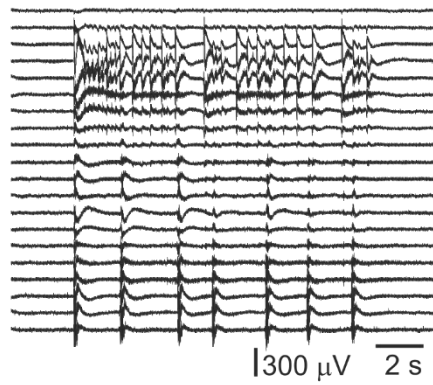
**C** NoEpi Complex-Simple
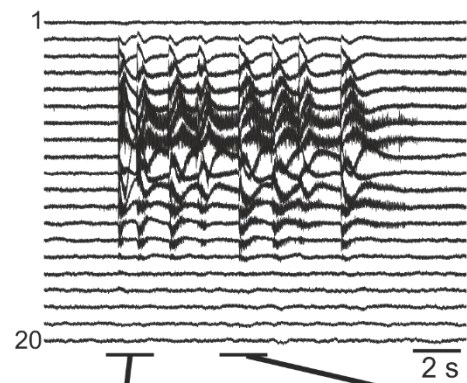
**D**
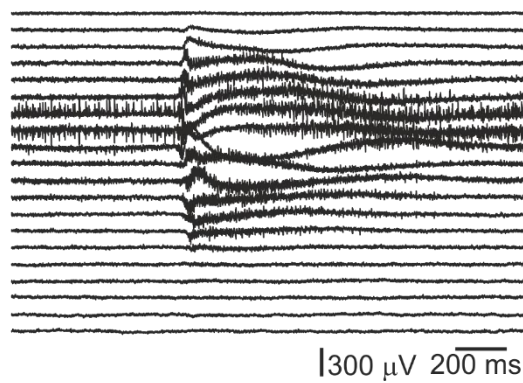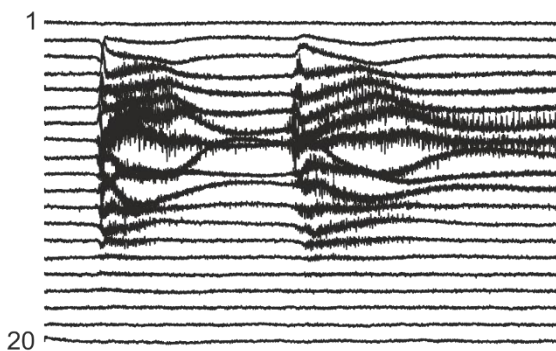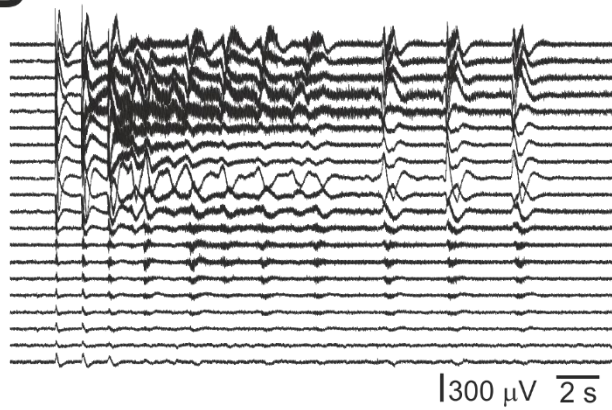
*Figure 3. BIC-induced seizures in the human neocortex*

During the application of BIC, long-lasting, seizure-like epileptiform events emerged spontaneously in slices from ResEpi (A, B) and NoEpi (C, D) tissue. They always invaded all (supragranular, granular and infragranular) layers of the neocortex and were temporally complex events. Most of them (n=5/7 in ResEpi and n=1/3 in NoEpi) were spatially complex epileptiform activities (A, see magnification in the second row), but spatially simple seizures (C, magnified on the bottom) were also detected. The length of the seizures varied between 15 and 28 seconds.
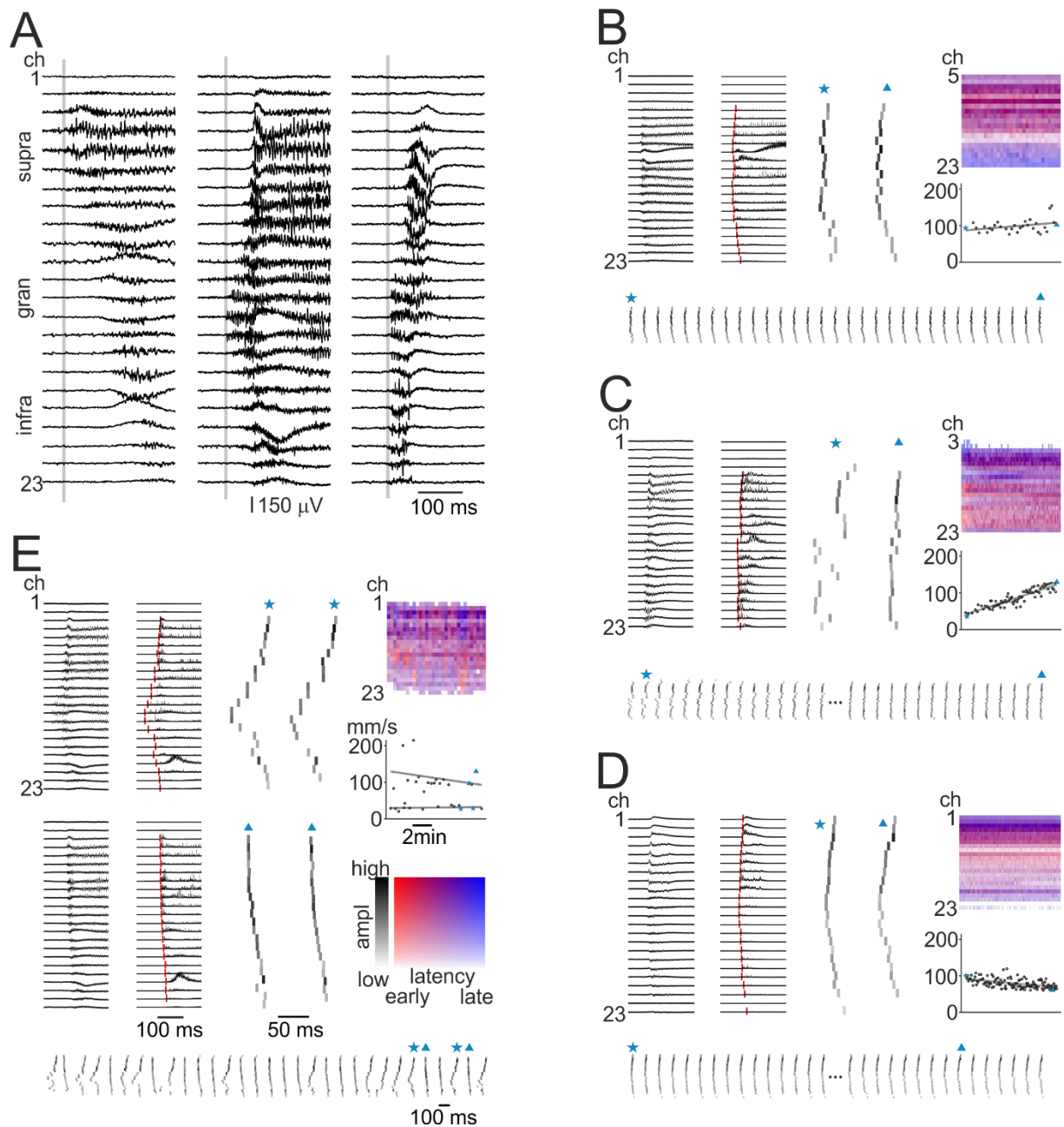
*Figure 4. Initiation and propagation of BIC-induced IISs within the neocortex*

A) IISs could be initiated in every layers of the human neocortex: supragranular (left panel), granular (middle panel) and infragranular (right panel) layers.

B-E) We determined the initiation region and the spreading direction of the recurring IISs. We detected the starting point of every IIS event on every channel (red lines on the second panel) and calculated the propagation speed of the events within the neocortical column (right panel, bottom). In each subfigure the left panel shows the original recording of an event, the second panel shows the absolute values with the starting points (red lines). On the bottom, the consecutive IIS events are visualized with the detected raster plots, two of which (marked with

blue star and triangle) are magnified in the middle panel. The colour intensity of the grey raster lines is in correlation with the LFPg amplitude of the event on that channel (colour scale is on subfigure E). The heat map in the right panel (top) illustrates the spreading speed of the IIS. Each column is an IIS event, each row corresponds to a channel. Red colours show the initiating channels, blue colours show the late activating channels. The intensity of the colours is related to the LFPg amplitude of the event on the given channel (colour scale is on subfigure E). The propagation speed (right panel, bottom) was stable in most of the cases (B) but increasing (C) or decreasing (D) speed was also observed. Two types of IIS with different propagation patterns (E, blue star and blue triangle) were simultaneously occurring in two recordings (one from ResEpi, one from NoEpi). The change in the propagation speed was often related to the modification in the jitter of channel activation (compare the event marked with the blue star to the event marked with the blue triangle on subfigure C).
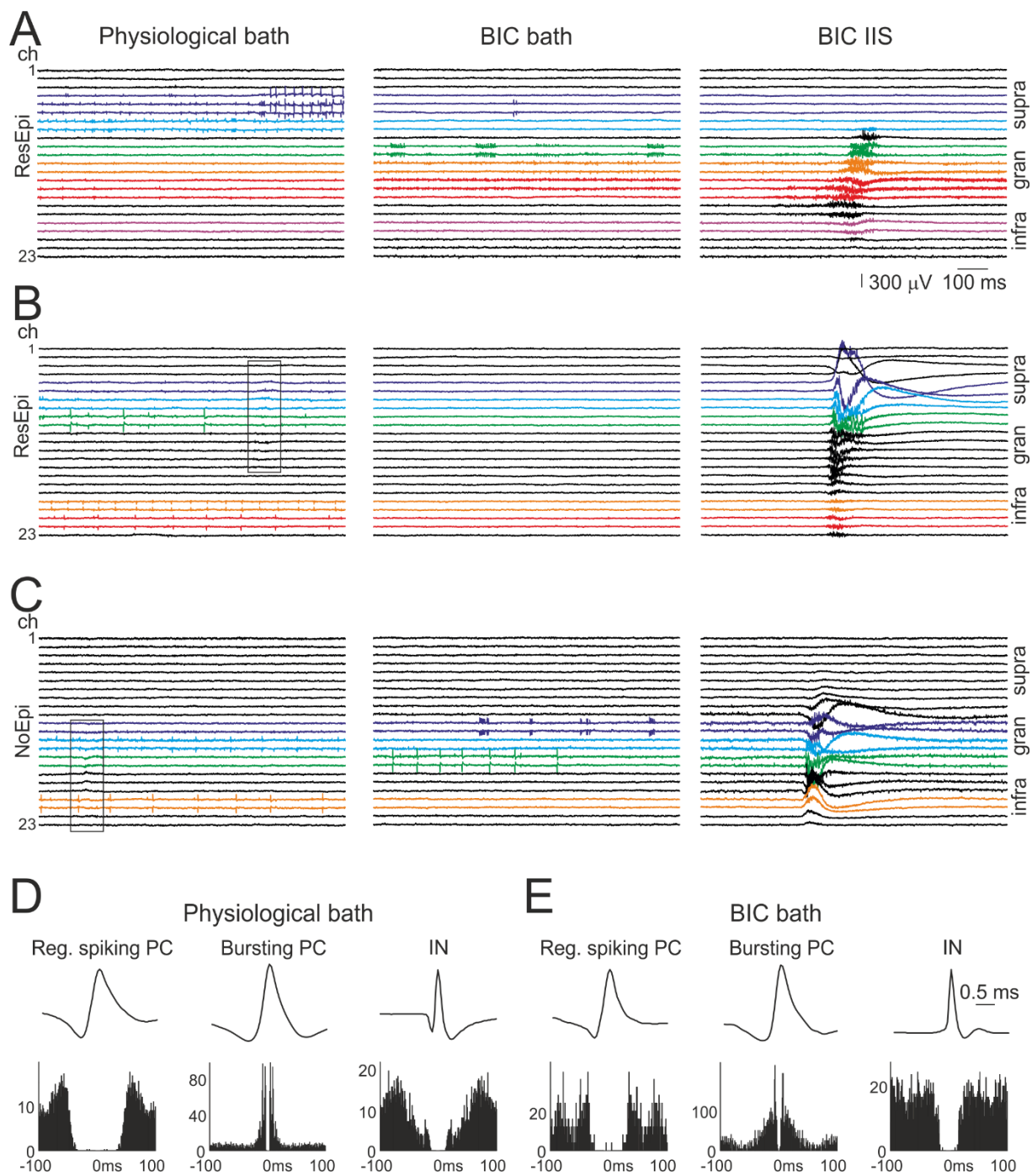
*Figure 5. The effect of BIC on action potentials*

A-C: Single cell firing during the application of physiological solution (left panels) and BIC bath (middle and right panels). Black rectangles indicate SPAs on the left panels (note the difference in amplitude compared to IISs on the right panels. Same scales apply to all subfigures). Spontaneously occurring neuronal discharges were observed mainly in the supragranular and infragranular layer in physiological solution. In contrast, in the presence of BIC, the majority of these cells became silent (for example cells on the dark and light blue, as

well as the orange and red channels on A; all cells on B; and cells on the light blue and orange channels on C). In addition, other neurons started to spontaneously discharge (see green, orange and purple channels on A, dark blue and green channels on C). Several (mainly granular) cells showed a characteristic bursting-like behaviour (green channel on A, dark blue channel on C). In several slices, most of the cells stayed silent when applying BIC, and showed excessive discharges only during the IISs (B).

D-E: Interneurons, bursting principal cells and regularly spiking principal cells were identified by the shape of their action potentials and the autocorrelogram of their firing. These characteristics remained unchanged in the presence of BIC (E).
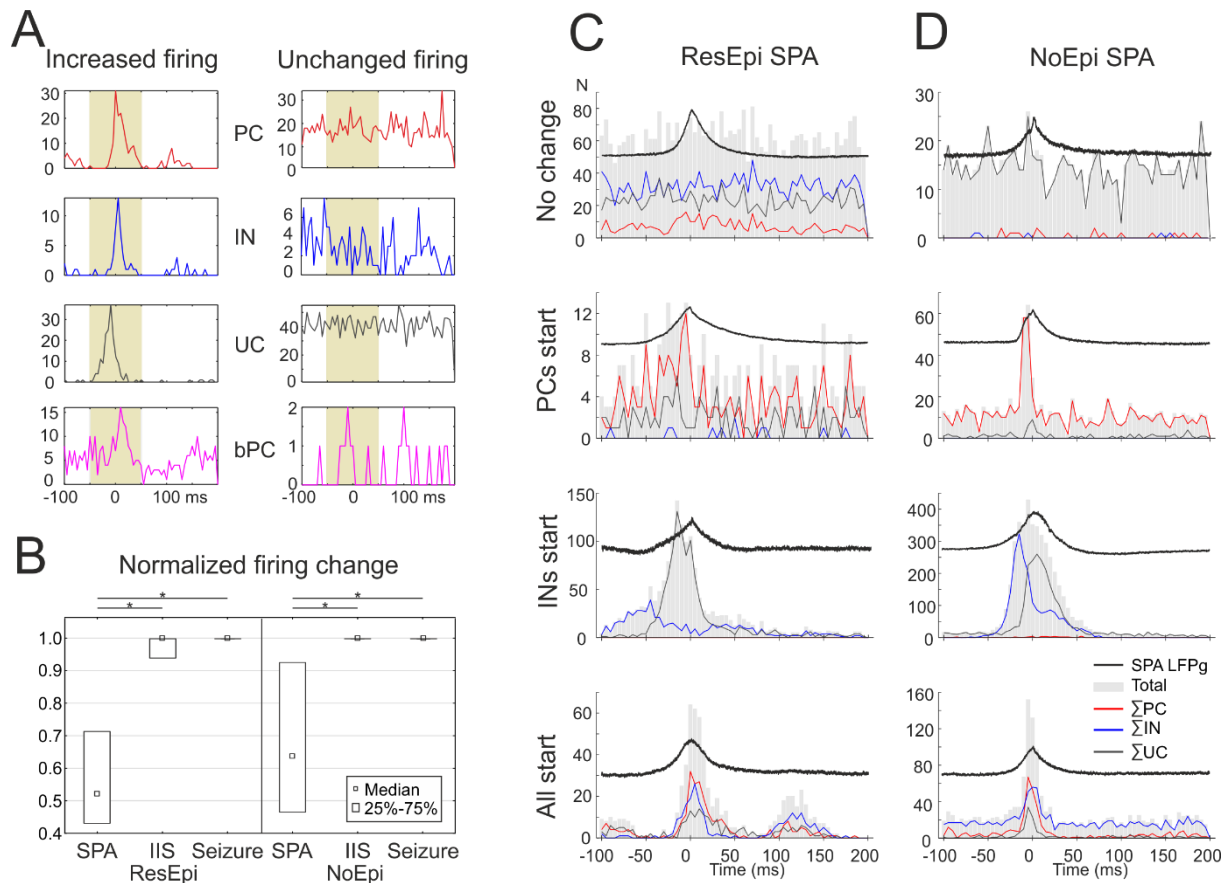
*Figure 6. Single cell firing during SPA*

A) Examples of single cell PETHs showing increased and unchanged firing during SPA (red: PC, blue: IN, grey: UC, purple: intrinsically bursting PC). Yellow shading shows the period of ±50 ms around the LFPg peak of the SPA.

B) The normalized firing change of all cells was significantly different during SPAs, IISs and seizures, both in the ResEpi and the NoEpi groups.

Different initiation patterns were observed during SPAs. In 40% and 36% of the cases in ResEpi (C) and NoEpi (D) slices, respectively, no single cell firing increase was observed (first row). In 13% (ResEpi) and 21% (NoEpi) of the cases PCs started to discharge while other cell types followed (second row), while INs initiated in 27% in ResEpi and in 21% in NoEpi slices (third row). Other patterns were also observed, for example the simultaneous firing increase of all cell types (bottom row).

A **PC start**

B **IN start**

C **UC start**

D

E

PC
bursting PC
IN
UC
Total

100 ms
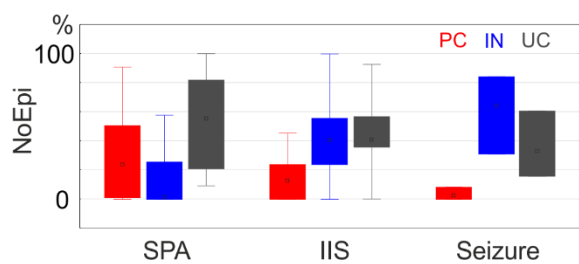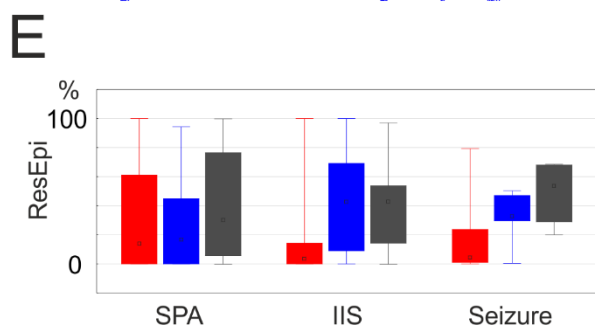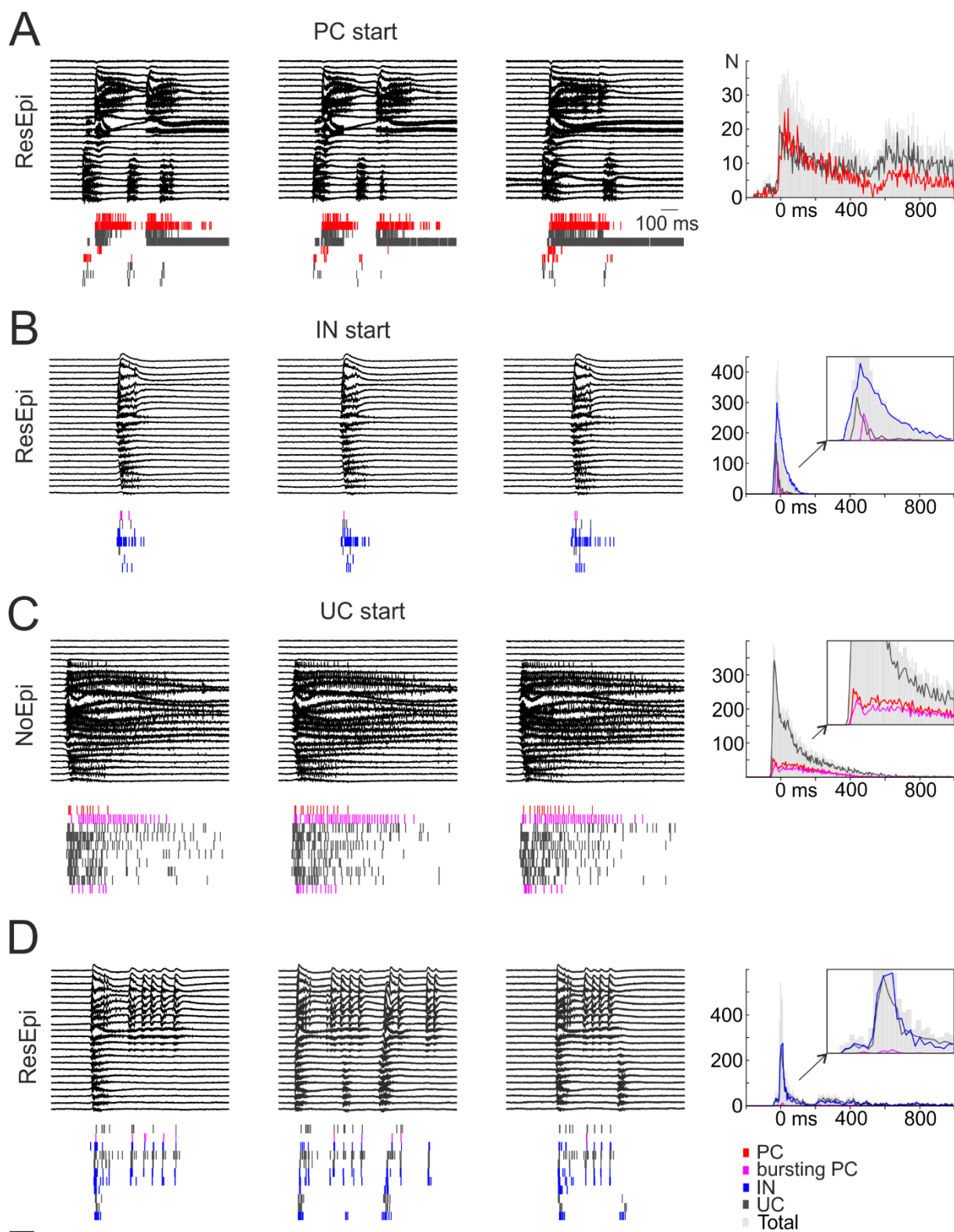
*Figure 7. Single-cell behaviour during IIS*

We observed different kinds of initiation patterns regarding the firing increase during IISs. Peri-event time histograms were calculated for all PCs (red), INs (blue) and UCs (grey) related to IIS events (right panels). Contrary to our expectations, PC firing increase at the start (A) was seen only in a minority of the cases (21% in ResEpi, 15% in NoEpi). Our observation was that INs preceded the discharge of other cell types (B) in most cases (50% in ResEpi, 38% in NoEpi). In some instances, UC cells (D) or UC cells together with INs (D) started to fire and the other cells followed (29% in ResEpi, 46% in NoEpi). The firing of intrinsically bursting PCs (purple on B, C, D) always followed the activation of other cells detected in the same recording. Below the single sweeps, raster plots show the firing of the cells clustered in the given recording. Note the variability in single cell firing during consecutive events. In case of spatially complex IISs (A, D) cell discharge was associated to the activation pattern of the neocortical layers. E) Contribution of PC (red) and IN (blue) discharge to the total cell firing during SPAs, IISs and seizures in ResEpi (left) and NoEpi (right) samples. PCs had higher impact on the overall firing during SPAs, than INs, whereas IN firing was considerably more pronounced than PC firing during both IISs and seizures.

Table 1. Patient data

| Stage of epilepsy | Patients | Gender | Age | Histology/Diagnosis | Resected cortical region | Duration of epilepsy | Distance from tumour | Anatomy of obtained tissue |
|---|---|---|---|---|---|---|---|---|
| ResEpi | E2 | F | 21 | focal cortical dysplasia with glioneural heterotopia | frontal | 2 years | | dysgenetic |
| ResEpi | E3 | F | 18 | bilateral frontal polymicrogyria | frontal | 5 years | | dysgenetic |
| ResEpi | E4 | M | 24 | ganglioglioma grade I | temporal | 4 years | distant | normal |
| ResEpi | E5 | F | 18 | focal cortical dysplasia II B | temporal | 5 years | | dysgenetic |
| ResEpi | E23 | F | 33 | haemangioma cavernosum | temporal | 5 years | | normal |
| ResEpi | E27 | M | 27 | hippocampal sclerosis | temporal | 2 years | | normal |
| ResEpi | E29 | M | 18 | focal cortical dysplasia | parietal | 5 years | | dysgenetic |
| ResEpi | E30 | M | 30 | microdysgenesis + hippocampal sclerosis | temporal | 17 years | | dysgenetic |
| ResEpi | E32 | F | 31 | focal cortical dysplasia II B (with balloon cells) | parietal | 18 years | | dysgenetic |
| ResEpi | E34 | F | 18 | ganglioglioma grade I + hippocampal sclerosis | temporal | 4 years | distant | N/A |
| ResEpi | E35 | F | 37 | cavernous malformation | temporal | 6 years | | N/A |
| ResEpi | E51 | M | 29 | cortical dysplasia | temporal | 14 years | | dysgenetic |
| ResEpi | E57 | F | 19 | focal cortical dysplasia II B (with balloon cells) | frontal | 15 years | | dysgenetic |
| ResEpi | E58 | F | 35 | haemangioma cavernosum | temporal | 5 years | | normal |
| ResEpi | E59 | M | 30 | focal cortical dysplasia II B (with balloon cells) | parietal | 27 years | | normal |
| ResEpi | E63 | M | 34 | diffuse low-grade glioneural tumor + hippocampal sclerosis | temporal | 20 years | close | infiltrated |
| ResEpi | E64 | M | 32 | focal cortical dysplasia II B (with balloon cells and dysmorph neurons) | parietal | 23 years | | normal |
| ResEpi | E65 | F | 31 | ganglioglioma grade I | temporal | 1 year | close | normal |
| ResEpi | E66 | F | 41 | hippocampal and temporal gliosis | temporal | 9 years | | normal |
| ResEpi | HP1 | M | 36 | temporal gliosis | temporal | 7 years | | normal |
| | | | | | | | | |
| TreatEpi | T5 | F | 35 | oligodendroglioma grade III | occipital | 1 month (1 seizure) | close | infiltrated |
| TreatEpi | T9 | F | 48 | lung small cell carcinoma metastaticum | occipital | 2 weeks (1 status epilepticus) | close | infiltrated |
| TreatEpi | T10 | M | 44 | glioblastoma multiforme, astrocytoma grade IV | temporal | 3 weeks | distant | normal |
| TreatEpi | T34 | F | 64 | haematoma | frontal | 1 week (1 seizure) | distant | N/A |
| TreatEpi | T46 | F | 68 | glioblastoma multiforme grade IV | temporal | postoperative | close | normal |
| | | | | | | | | |

| | | | | | | | | |
|---|---|---|---|---|---|---|---|---|
| NoMed | E26 | M | 44 | anaplastic ganglioglioma grade III | temporal | 3 months (1 seizure) | distant | N/A |
| NoMed | E33 | M | 63 | lung adenocarcinoma metastaticum | occipital | 2 weeks (1 seizure) | close | N/A |
| NoMed | E44 | F | 32 | anaplastic astrocytoma grade III | frontal | N/A (1 seizure) | distant | N/A |
| NoMed | E56 | M | 58 | lung adenocarcinoma metastaticum | temporal | 10 months (1 seizure) | close | infiltrated |
| NoMed | E60 | F | 36 | anaplastic astrocytoma grade III | frontal | N/A (1 seizure) | close | infiltrated |
| | | | | | | | | |
| NoEpi | T4 | F | 69 | glioblastoma multiforme | temporal | | distant | normal |
| NoEpi | T6 | M | 31 | cavernoma, haematoma intracerebralis acuta | frontal | | distant | normal |
| NoEpi | T8 | F | 78 | glioblastoma multiforme, astrocytoma grade IV | temporal | | distant | normal |
| NoEpi | T11 | F | 57 | glioblastoma multiforme grade IV | occipital | | distant | normal |
| NoEpi | T17 | F | 74 | glioblastoma multiforme grade IV | parietal | | distant | normal |
| NoEpi | T32 | M | 79 | glioblastoma multiforme grade III | temporal | | close | N/A |
| NoEpi | T33 | M | 45 | anaplastic astrocytoma | frontal | | close | N/A |
| NoEpi | T36 | M | 58 | lung adenocarcinoma metastaticum | frontal | | close | N/A |
| NoEpi | T39 | M | 37 | centralis neurocytoma grade II | frontal | | distant | N/A |
| NoEpi | T56 | M | 64 | glioblastoma multiforme grade IV | parietal | | close | normal |
| NoEpi | T57 | F | 73 | glioblastoma multiforme grade IV | frontal | | close | infiltrated |
| NoEpi | T58 | M | 42 | glioblastoma multiforme grade IV | frontal | | close | normal |
| NoEpi | T61 | F | 40 | anaplastic astrocytoma grade III | parietal | | distant | normal |
| NoEpi | T64 | M | 63 | glioblastoma multiforme grade IV | parietal | | close | normal |
| NoEpi | T67 | F | 57 | glioblastoma multiforme grade IV | parietal | | close | normal |
| NoEpi | T68 | F | 72 | neuroendocrine carcinoma metastaticum, grade III | parietal | | distant | normal |
| NoEpi | T69 | M | 49 | anaplastic astrocytoma grade III | frontal | | distant | N/A |
| NoEpi | HP3 | M | 55 | epithelial lung carcinoma metastaticum | temporal | | distant | normal |
| NoEpi | HP4 | M | 69 | planocellular keratoid carcinoma metastaticum | occipital | | close | N/A |

F=female, M=male, N/A=not available, Stage of epilepsy: ResEpi: pharmacoresistant epilepsy, TreatEpi: treatable epilepsy, NoMed: no need for medication, NoEpi: no epilepsy. Distance from the tumour: close is <3 cm, distant is >3 cm, but in most cases >5 cm.

Table 2.
Number of slices generating bicuculline-induced activity. We distinguished four categories based on the presence/absence of SPAs in physiological bath solution and the subsequent presence/absence of BIC-induced activity. All Epi=ResEpi+TreatEpi+NoMed

| Slices | All Epi | ResEpi | TreatEpi | NoMed | NoEpi |
|---|---|---|---|---|---|
| SPA – BIC event (n) | 19 (44.2%) | 16 (55.2%) | 3 (33.3%) | 0 (0.0%) | 12 (46.2%) |
| no SPA – BIC event (n) | 8 (18.6%) | 5 (17.2%) | 1 (11.1%) | 2 (40.0%) | 3 (11.5%) |
| SPA – no BIC event (n) | 7 (16.3%) | 3 (10.4%) | 3 (33.3%) | 1 (20.0%) | 8 (30.8%) |
| no SPA – no BIC event (n) | 9 (20.9%) | 5 (17.2%) | 2 (22.2%) | 2 (40.0%) | 3 (11.5%) |
| **Total slices (n)** | **43** | **29** | **9** | **5** | **26** |

Table 3.
Distribution of bicuculline-induced epileptiform activities across the different patient groups.

| | Temporal complexity | Spatial complexity | ResEpi Activities n (%) | TreatEpi Activities n (%) | NoMed Activities n (%) | NoEpi Activities n (%) |
|---|---|---|---|---|---|---|
| Interictal spike (entire) | simple | simple | 7 (22.6%) | 3 (30%) | 1 (16.7%) | 13 (48.2%) |
| | complex | simple | 1 (3.2%) | 1 (10%) | | |
| | complex | complex | 2 (6.5%) | | | |
| Interictal spike (supra-gran) | simple | simple | 2 (6.5%) | | | |
| | complex | simple | 2 (6.5%) | | | |
| Interictal spike (gran-infra) | simple | simple | 2 (6.5%) | | | |
| Seizure | complex | simple | 2 (6.5%) | 1 (10%) | 1 (16.7%) | 2 (7.4%) |
| | complex | complex | 5 (16.1%) | | | 1 (3.7%) |
| No BIC-induced event | | | 8 (25.7%) | 5 (50%) | 4 (66.6%) | 11 (40.7%) |
| **Total (n)** | | | **31** | **10** | **6** | **27** |

entire= involving the entire width of the neocortex, supra-gran=involving supragranular+granular layers, gran-infra=involving granular+infragranular layers

Table 4.
Characteristics of SPAs, bicuculline-induced IISs and seizures.
All data are provided in median [1st and 3rd quartile] and in (mean±standard deviation)
n.s.: not significant, N/A: not applicable

| Patient group | Population activity (number of slices) | Recurrence frequency (Hz) | Duration (SPA: ms, IIS, seizure: s) | Maximal LFPg amplitude (μV) | Maximal MUA amplitude (μV) |
|---|---|---|---|---|---|
| ResEpi | SPA (n=21) | 0.74 [0.46 1.10] Hz (0.81±0.54 Hz) | 67.2 [46.8 86.2] ms (68.8±36.6 ms) | 31.65 [21.80 45.51] (38.76±23.67) | 0.83 [0.41 1.24] (1.28±1.28) |
| | IIS (n=16) | 0.012 [0.003 0.102] Hz (0.087±0.150 Hz) 0.75 [0.19 6.11] min$^{-1}$ (5.23±9.03 min$^{-1}$) | 0.30 [0.17 0.50] s (0.36±0.23 s) | 200.60 [133.66 295.71] (262.98±241.37) | 9.87 [5.64 20.23] (12.80±8.27) |
| | seizure (n=7) | 0.003 [0.003 0.008] Hz (0.007±0.007 Hz) 0.20 [0.18 0.46] min$^{-1}$ (0.42±0.42 min$^{-1}$) | 23.88 [18.05 25.27] s (21.75±4.44 s) | 485.87 [399.86 624.18] (526.24±259.06) | 14.96 [13.73 18.60] (16.35±5.47) |
| NoEpi | SPA (n=22) | 1.04 [0.62 1.39] Hz (1.08±0.64 Hz) | 40.7 [27.7 49.0] ms (41.6±18.9 ms) | 18.91 [14.04 36.57] (26.97±19.03) | 0.77 [0.49 1.22] (1.27±1.43) |
| | IIS (n=13) | 0.003 [0.002 0.031] Hz (0.015±0.018 Hz) 0.21 [0.10 1.89] 0.88±1.09 min$^{-1}$ | 0.48 [0.32 0.58] s (0.44±0.16 s) | 296.84 [124.85 463.91] (348.32±322.49) | 20.18 [19.56 27.73] (22.38±7.49) |
| | seizure (n=3) | 0.002 [0.002 0.003] Hz (0.002±0.001 Hz) 0.12 [0.11 0.16] min$^{-1}$ (0.14±0.05 min$^{-1}$) | 22.50 [22.19 25.35] s (24.19±3.48 s) | 839.97 [764.34 925.98] (847.09±161.46) | 36.59 [32.61 41.19] (37.01±8.59) |

| | | | | | |
|---|---|---|---|---|---|
| Significant differences between ResEpi and NoEpi | | n.s. | SPA ResEpi>NoEpi, p<0.01 | n.s. | IIS ResEpi<NoEpi, p<0.05 Seizure ResEpi<NoEpi p<0.01 |
| Significant differences between activity types (SPA-IIS-seizure) | | SPA frequency > IIS frequency, seizure frequency, p<0.0001 | N/A | SPA amplitude < IIS amplitude < seizure amplitude, p<0.0001 | SPA MUA < IIS MUA, seizure MUA, p< 0.0001 |

Table 5.
High frequency oscillatory activity during SPAs and IISs.
All data are provided in median [1st and 3rd quartile] and in (mean±standard deviation), n.s.: not significant

| | Synchronous activity | Number of SPAs/IISs with increased ripple activity | Number of SPAs/IISs with increased fast ripple activity | Ripple power (dB) | Ripple frequency (Hz) | Fast ripple power (dB) | Fast ripple frequency (Hz) |
|---|---|---|---|---|---|---|---|
| ResEpi | SPA (n=19) | 17 | 17 | 3.37 [2.38 4.67] (3.67±1.82) | 164.1 [152.3 193.4] (173.48±37.69) | 3.08 [2.07 3.87] (3.27±1.57) | 378.9 [372.1 490.2] (417.68±95.75) |
| | IIS (n=15) | 15 | 15 | 11.69 [9.84 16.30] (12.53±5.00) | 178.3 [159.2 211.4] (182.6±32.5) | 11.27 [9.80 15.65] (11.75±4.67) | 358.4 [339.6 403.3] (397.2±107.8) |
| TreatEpi | SPA (n=6) | 3 | 3 | 5.09 [3.03 5.96] (4.30±3.01) | 156.3 [150.4 208.1] (186.87±63.44) | 3.40 [2.33 4.45] (3.39±2.12) | 401.4 [366.7 491.3] (438.17±128.56) |
| | IIS (n=4) | 4 | 4 | 16.83 [13.57 20.07] (16.81±4.49) | 188.0 [179.9 204.6] (196.53±31.32) | 16.75 [14.82 17.69] (15.76±2.86) | 441.6 [419.0 479.0] (456.38±65.26) |
| NoMed | SPA - | - | - | - | - | - | - |
| | IIS (n=1) | 1 | 1 | 18.49 | 167.00 | 16.94 | 321.30 |
| NoEpi | SPA (n=22) | 17 | 14 | 2.60 [2.07 3.48] 3.09±1.59 | 203.1 [178.7 222.7] 198.3±33.3 | 2.73 [2.16 1.93] 3.07±1.60 | 487.3 [434.8 559.1] 492.6±107.7 |
| | IIS (n=13) | 11 | 11 | 16.54 [14.50 18.23] (16.05±3.32) | 206.1 [187.8 245.6] (215.57±47.21) | 16.11 [14.69 17.16] (15.77±3.30) | 429.7 [362.3 483.4] (444.43±109.04) |
| Significant differences between | | | | n.s. | n.s. | IIS NoEpi<ResEpi, TreatEpi p<0.05 | n.s. |

| patient groups | | | | | | | |
|---|---|---|---|---|---|---|---|
| Significant differences between activity types | | | | SPA ripple power < IIS ripple power, p<0.0001 | n.s. | SPA fast ripple power < IIS fast ripple power, p<0.0001 | n.s. |

Table 6. Characteristics of clustered single cells
Firing characteristics of clustered cells in physiological conditions (control) and during BIC application.

| | | Number of clustered cells | | Firing frequency (Hz) | | Interevent interval median (ms) | | Burstiness (% of APs within burst) | |
|---|---|---|---|---|---|---|---|---|---|
| | | Control | BIC | Control | BIC | Control | BIC | Control | BIC |
| ResEpi | **Total** | **193** | **191** | **0.21 [0.07 0.70] (1.01±2.78)** | **0.17 [0.05 0.69] (0.82±1.68)** | **0.18 [0.05 0.84] (3.86±16.18)** | **0.03 [0.01 0.15] (1.80±7.48)** | **0.00 [0.00 0.07] (0.06±0.12)** | **0.15 [0.00 0.39] (0.23±0.23)** |
| | PC | 76 (39.4%) | 28 (14.7%) | 0.19 [0.06 0.67] (1.11±2.85) | 0.19 [0.05 0.51] (0.48±0.78) | 0.11 [0.04 0.58] (4.91±21.46) | 0.02 [0.01 0.79] (4.44±12.61) | 0.00 [0.00 0.17] (0.08±0.14) | 0.14 [0.00 0.22] (0.15±0.19) |
| | IN | 38 (19.7%) | 69 (36.1%) | 0.33 [0.07 1.27] (0.91±1.23) | 0.22 [0.09 1.12] (1.20±2.36) | 0.38 [0.17 1.23] (4.83±15.62) | 0.02 [0.01 0.12] (1.25±3.96) | 0.00 [0.00 0.00] (0.03±0.07) | 0.15 [0.00 0.41] (0.23±0.24) |
| | UC | 79 (40.9%) | 94 (49.2%) | 0.22 [0.08 0.58] (0.96±3.23) | 0.13 [0.04 0.62] (0.65±1.17) | 0.12 [0.04 0.97] (2.40±9.03) | 0.03 [0.01 0.15] (1.41±7.36) | 0.00 [0.00 0.07] (0.05±0.11) | 0.18 [0.04 0.41] (0.25±0.23) |
| NoEpi | **Total** | **182** | **167** | **0.20 [0.06 0.52] (0.70±1.39)** | **0.17 [0.05 0.65] (0.64±1.38)** | **0.23 [0.07 1.61] (2.11±5.47)** | **0.01 [0.01 0.06] (1.82±10.91)** | **0.00 [0.00 0.07] (0.08±0.17)** | **0.16 [0.01 0.41] (0.25±0.26)** |
| | PC | 50 (27.5%) | 30 (18.0%) | 0.12 [0.05 0.80] (0.87±1.73) | 0.18 [0.04 0.87] (0.77±1.59) | 0.09 [0.04 0.23] (0.68±2.05) | 0.03 [0.01 0.18] (2.78±8.31) | 0.05 [0.00 0.13] (0.10±0.14) | 0.11 [0.00 0.28] (0.15±0.17) |
| | IN | 39 (21.4%) | 56 (33.5%) | 0.22 [0.06 0.47] (0.65±1.23) | 0.14 [0.05 0.34] (0.58±1.07) | 1.43 [0.30 3.89] (4.09±6.26) | 0.01 [0.00 0.04] (0.41±1.54) | 0.00 [0.00 0.00] (0.04±0.12) | 0.18 [0.01 0.54] (0.30±0.31) |
| | UC | 93 (51.1%) | 81 (48.5%) | 0.21 [0.08 0.47] (0.62±1.25) | 0.19 [0.05 0.68] (0.63±1.50) | 0.26 [0.07 1.45] (2.06±6.13) | 0.01 [0.01 0.04] (2.43±14.78) | 0.00 [0.00 0.05] (0.09±0.20) | 0.19 [0.03 0.34] (0.24±0.24) |
| Significant differences between patient groups | | n.s. | n.s. | | | ResEpi IN < NoEpi IN p<0.05 | ResEpi Total > NoEpi Total | n.s. | n.s. |

| | | | | p<0.001;<br>ResEpi IN ><br>NoEpi IN<br>p<0.0001<br>ResEpi UC ><br>NoEpi UC<br>p<0.0001 | | |
|---|---|---|---|---|---|---|
| Significant differences between cell types | n.s. | n.s. | ResEpi PC<IN<br>p<0.01<br>ResEpi PC<UC<br>p<0.05<br>NoEpi PC<UC<IN<br>p<0.0001 | NoEpi PC>IN<br>p<0.001<br>NoEpi PC>UC<br>p<0.05 | ResEpi IN<PC<br>p<0.05<br>NoEpi IN<PC<br>p<0.001 | n.s. |
| Significant differences between control and BIC | n.s. | | ResEpi Total control > BIC p<0.0001<br>NoEpi Total control > BIC p<0.0001<br>ResEpi IN control > BIC p<0.0001<br>ResEpi UC control > BIC p<0.0001<br>NoEpi IN control > BIC p<0.0001<br>NoEpi UC control > BIC p<0.0001 | | ResEpi Total control < BIC p<0.0001<br>NoEpi Total control < BIC p<0.0001<br>ResEpi PC control < BIC p<0.05<br>ResEpi IN control < BIC p<0.0001<br>ResEpi UC control < BIC p<0.0001<br>NoEpi IN control < BIC p<0.0001<br>NoEpi UC control < BIC p<0.0001 | |

Table 7. Normalized firing change of cells during SPA/IIS/seizures. This was calculated in the form of A/A+B, where A is the firing frequency (number of APs/sec) falling into the time window of the events, and B is the firing frequency during the baseline period. A cell was considered to have an increased firing if its normalized firing change was equal or more than 0.6 (increase to ≥150%).

| | ResEpi | | | NoEpi | | |
|---|---|---|---|---|---|---|
| | SPA | IIS | Seizure | SPA | IIS | Seizure |
| **Total N of cells** | **136** | **138** | **72** | **124** | **129** | **38** |
| **N of cells with increased firing** | **53 (39%)** | **119 (86%)** | **71 (99%)** | **69 (56%)** | **123 (95%)** | **38 (100%)** |
| **Normalized firing change of all cells** | **0.52 [0.43-0.71] (0.55±0.30)** | **1.0 [0.94-1.0] (0.86±0.31)** | **1.0 [1.0-1.0] (0.97±0.12)** | **0.64 [0.46-0.92] (0.64±0.31)** | **1.0 [1.0-1.0] (0.95±0.17)** | **1.0 [1.0-1.0] (1.0±0.00)** |
| N of PCs | 44 | 19 | 21 | 34 | 28 | 2 |
| N of PCs with increased firing | 18 (41%) | 17 (90%) | 20 (95%) | 17 (50%) | 26 (93%) | 2 (100%) |
| Normalized firing change of PCs | 0.52 [0.34-0.71] (0.50±0.33) | 1.0 [0.91-1.0] (0.89±0.25) | 1.0 [1.0-1.0] (0.95±0.22) | 0.59 [0.44-0.78] (0.60±0.30) | 1.0 [1.0-1.0] (0.94±0.20) | 1.0 [1.0-1.0] (1.0±0.00) |
| N of bursting PCs | 3 | 4 | 0 | 5 | 3 | 0 |
| N of bursting PC with increased firing | 2 (67%) | 3 (75%) | 0 | 2 (40%) | 3 (100%) | 0 |
| Normalized firing change of bursting PCs | 0.60 [0.57-0.62] (0.59±0.03) | 1.0 [1.0-1.0] (1.0±0.00) | - | 0.67 [0.40-0.73] (0.55±0.36) | 1.0 [0.92-1.0] (0.97±0.05) | - |
| N of INs | 35 | 49 | 21 | 28 | 33 | 23 |
| N of INs with increased firing | 11 (31%) | 42 (86%) | 21 (100%) | 16 (57%) | 33 (100%) | 23 (100%) |
| Normalized firing change of INs | 0.50 [0.47-0.65] (0.52±0.23) | 1.0 [0.97-1.0] (0.88±0.27) | 1.0 [1.0-1.0] (0.98±0.04) | 0.72 [0.37-0.94] (0.62±0.34) | 1.0 [1.0-1.0] (0.98±0.08) | 1.0 [1.0-1.0] (1.0±0.00) |
| N of UCs | 57 | 70 | 30 | 62 | 68 | 13 |
| N of UCs with increased firing | 24 (42%) | 60 (86%) | 30 (100%) | 36 (58%) | 64 (94%) | 13 (100%) |
| Normalized firing change of UCs | 0.56 [0.43-0.88] (0.58±0.32) | 1.0 [0.94-1.0] (0.83±0.35) | 1.0 [1.0-1.0] (0.98±0.06) | 0.64 [0.50-0.93] (0.66±0.30) | 1.0 [1.0-1.0] (0.95±0.19) | 1.0 [1.0-1.0] (1.0±0.00) |

| Significant differences in the normalized firing change between synchronous activity types | ResEpi SPA<IIS, p<0.0001<br>ResEpi SPA<seizure, p<0.0001 | | | NoEpi SPA<IIS, p<0.0001<br>NoEpi SPA<seizure, p<0.0001 | | |
|---|---|---|---|---|---|---|
| Significant differences between patient groups | n.s. | n.s. | n.s. | n.s. | n.s. | n.s. |
| Significant differences in the firing change between cell types | n.s. | n.s. | n.s. | n.s. | n.s. | n.s. |

Table 8. Contribution of excitatory and inhibitory firing during SPAs and the initiation phase of IISs and seizures. We calculated the percentage of PC/IN/UC APs relative to the total number of APs in the time window of the SPA events (-50 to +50 ms), or at the initial phase (-100 to +200 ms) of IISs and seizures.

| | ResEpi | | | NoEpi | | |
|---|---|---|---|---|---|---|
| | SPA (n=15) | IIS (n=15) | Seizure (n=6) | SPA (n=14) | IIS (n=13) | Seizure (n=3) |
| Contribution of PC firing (%) | 13.9 [0.0-61.1] (32.7±36.7) | 3.6 [0.0-14.4] (16.5±29.0) | 4.4 [1.1-23.8] (18.8±30.9) | 23.9 [1.1-50.7] (31.7±33.2) | 12.6 [0.0-23.8] (14.2±16.4) | 2.6 [0.0-8.3] (3.6±4.3) |
| Contribution of bursting PC firing (%) | 0.0 [0.0-0.0] (3.9±13.1) | 0.0 [0.0-1.0] (1.7±3.7) | - | 0.0 [0.0-8.6] (7.2±14.7) | 0.0 [0.0-0.0] (1.4±3.9) | - |
| Contribution of IN firing (%) | 16.8 [0.0-44.8] (24.3±30.8) | 42.5 [9.1-69.2] (43.4±34.3) | 32.8 [29.7-47.1] (32.2±17.7) | 1.4 [0.0-25.7] (15.4±21.5) | 40.7 [23.8-55.8] (43.3±29.7) | 64.3 [31.1-84.2] (59.9±26.8) |
| Contribution of UC firing (%) | 30.2 [6.0-76.6] (43.0±37.8) | 43.1 [14.5-54.0] (40.1±28.7) | 53.7 [29.1-68.3] (49.0±20.4) | 55.4 [20.8-81.8] (52.9±33.5) | 40.7 [35.7-56.8] (42.6±28.2) | 33.0 [15.8-60.6] (36.5±22.6) |
| Significant differences | n.s. | | | NoEpi SPA IN < NoEpi IIS IN, p<0.05 | | |